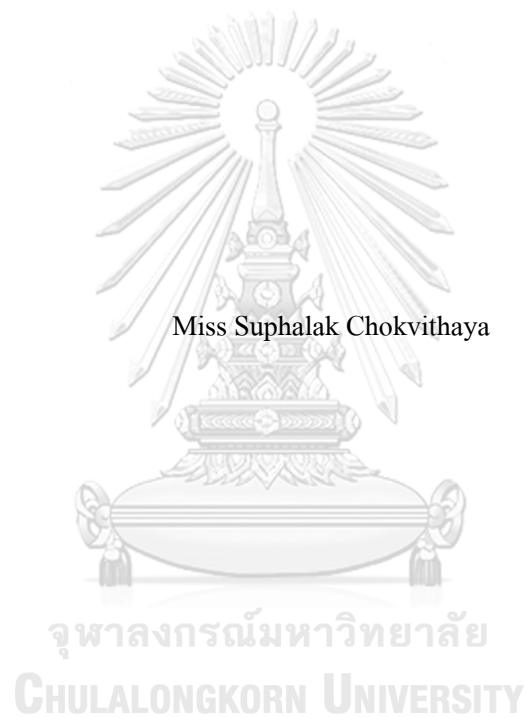


Functional studies of p.N258K and p.G279D variants in the *KCNQ2* gene



A Thesis Submitted in Partial Fulfillment of the Requirements
for the Degree of Master of Science in Medical Sciences

FACULTY OF MEDICINE

Chulalongkorn University

Academic Year 2022

Copyright of Chulalongkorn University

การศึกษาการทำงานของกรกลายพันธุ์ p.N258K และ p.G279D ในยีน KCNQ2



วิทยานิพนธ์นี้เป็นส่วนหนึ่งของการศึกษาตามหลักสูตรปริญญาวิทยาศาสตรมหาบัณฑิต
สาขาวิชาวิทยาศาสตร์การแพทย์ไม่สังกัดภาควิชา/เทียบเท่า
คณะแพทยศาสตร์ จุฬาลงกรณ์มหาวิทยาลัย
ปีการศึกษา 2565
ลิขสิทธิ์ของจุฬาลงกรณ์มหาวิทยาลัย

Thesis Title Functional studies of p.N258K and p.G279D variants in the
KCNQ2 gene
By Miss Suphalak Chokvithaya
Field of Study Medical Sciences
Thesis Advisor Professor VORASUK SHOTELERSUK, M.D.
Thesis Co Advisor Associate Professor SAKNAN BONGSEBANDHU-
 PHUBHAKDI, Ph.D.

Accepted by the FACULTY OF MEDICINE, Chulalongkorn University in Partial
Fulfillment of the Requirement for the Master of Science

..... Dean of the FACULTY OF MEDICINE
(Associate Professor CHANCHAI SITTIPUNT, M.D.)

THESIS COMMITTEE

..... Chairman
(Professor APIWAT MUTIRANGURA, M.D., Ph.D.)

..... Thesis Advisor
(Professor VORASUK SHOTELERSUK, M.D.)

..... Thesis Co-Advisor
(Associate Professor SAKNAN BONGSEBANDHU-
PHUBHAKDI, Ph.D.)

..... Examiner
(Associate Professor WILAI ANOMASIRI, Ph.D.)

..... External Examiner
(Associate Professor THIPWIMOL TIM-AROON, M.D.)

ศุภลักษณ์ โชควิทยา : การศึกษาการทำงานของการกลายพันธุ์ p.N258K และ p.G279D ในยีน KCNQ2 . (Functional studies of p.N258K and p.G279D variants in the *KCNQ2* gene) อ.ที่ปรึกษาหลัก : ศ.วรศักดิ์ โชติเลอศักดิ์, อ.ที่ปรึกษาร่วม : รศ. ดร.ศกนัน พงศ์พันธุ์ผู้ภักดี

การกลายพันธุ์ในยีน *KCNQ2* มีความสัมพันธ์กับ โรคลมชักในเด็กที่มีอาการตั้งแต่แรกเกิด (Infantile-onset epileptic disorders) ซึ่งอาการชักทางคลินิกมีความแตกต่างกันตั้งแต่ความรุนแรงน้อย (Self-limited neonatal seizures) สามารถกลับมาเป็นปกติได้เอง ไปจนถึงมีความรุนแรงมากนั่นคือ ไข้สมองอักเสบจากโรคลมชักและมักจะมีพัฒนาการทางสมองล่าช้าร่วมด้วย (epileptic encephalopathy and delayed development) การกลายพันธุ์นี้มีผลต่อการทำงานของช่องโพแทสเซียม (Potassium channel ชนิด Kv7.2) ซึ่งมีทำงานมากกว่าปกติหรือน้อยกว่าปกติ แต่จะมีอาการชักเหมือนกัน เพื่อให้เข้าใจความสัมพันธ์ของจีโนมไทป์และฟีโนไทป์ได้ดียิ่งขึ้น จำเป็นต้องศึกษาเพิ่มเติมถึงการกลายพันธุ์ของผู้ป่วยในกลุ่มโมเดลที่ชัดเจนเพื่อเป็นแนวทางในการรักษา ในการศึกษาที่เรารายงานผู้ป่วยที่ไม่เกี่ยวข้องกัน 9 รายที่เป็น โรคลมชักที่เกี่ยวข้องกับ ยีน *KCNQ2* ซึ่งพบว่ามีการกลายพันธุ์ p.N258K และ p.G279D ในผู้ป่วย 2 ราย ที่ไม่เคยมีการรายงานมาก่อน มีลักษณะถ่ายทอดทางพันธุกรรมแบบ de novo heterozygous จากการตรวจ whole exome sequencing (WES) นำมาตรวจสอบกลไกระดับโมเลกุลโดยใช้เทคนิคทางสรีรวิทยาไฟฟ้า (Electrophysiological techniques) ร่วมกับการวิเคราะห์การแสดงออกของโปรตีนที่เชื่อมหุ้มผิวเซลล์โดยพบว่า มีการแสดงออกน้อยลงทั้ง p.N258K และ p.G279D และผลการวิเคราะห์ทางไฟฟ้า พบว่าการกลายพันธุ์ทั้ง 2 แบบ ทำให้มีความเปลี่ยนแปลงไปจากปกติทั้ง กระแสไฟฟ้า และความหนาแน่นกระแสไฟฟ้าของช่องโพแทสเซียม Kv7.2 บทพร่องอย่างมีนัยสำคัญทางสถิติ การเปลี่ยนขั้วของการนำไฟฟ้าในการพึ่งพาแรงดันไฟฟ้าของการกระตุ้น ความต้านทานของเยื่อหุ้มผิวเซลล์และค่าคงที่เวลาในการเปลี่ยนศักย์ไฟฟ้าของเยื่อหุ้มผิวเซลล์ ซึ่งทั้งหมดนี้บ่งชี้ถึงการสูญเสียการทำงานในช่องโพแทสเซียม Kv7.2 ทั้งแบบ homotetrameric และ heterotetrameric ที่ทำงานร่วมกับช่องโพแทสเซียมชนิด Kv7.3 นอกจากนี้การกลายพันธุ์ทั้ง 2 แบบ ยังให้ผลเชิงลบที่โดดเด่น (dominant-negative effects) ในช่องโพแทสเซียม Kv7.2 แบบ heterotetrameric ดังนั้นจึงสรุปได้ว่า การกลายพันธุ์ p.N258K และ p.G279D ในยีน *KCNQ2* เป็นสาเหตุทำให้ช่องโพแทสเซียม Kv7.2 ทำงานได้น้อยลง ส่งผลทำให้เกิด โรคลมชักในวัยแรกเกิด

สาขาวิชา วิทยาศาสตร์การแพทย์
ปีการศึกษา 2565

ลายมือชื่อนิติ
ลายมือชื่อ อ.ที่ปรึกษาหลัก
ลายมือชื่อ อ.ที่ปรึกษาร่วม

6270021430 : MAJOR MEDICAL SCIENCES

KEYWORD: Developmental and epileptic encephalopathy (DEE); Self-limited neonatal seizures;
The KCNQ2 gene; whole-cell patch-clamp analysis.

Suphalak Chokvithaya : Functional studies of p.N258K and p.G279D variants in the
KCNQ2 gene. Advisor: Prof. VORASUK SHOTELERSUK, M.D. Co-advisor: Assoc.
Prof. SAKNAN BONGSEBANDHU-PHUBHAKDI, Ph.D.

Mutations in the *KCNQ2* gene encoding for voltage-gated K channel subunits underlying the neuronal M-current, have been associated with infantile-onset epileptic disorders. The clinical spectrum ranges from self-limited neonatal seizures to epileptic encephalopathy and delayed development. Although gain- and loss-of-function mutations of *KCNQ2* leads to indistinguishable phenotypes, different therapeutic approaches are required. To better understand genotype-phenotype correlation, more reports of patients and their mutations with elucidated molecular mechanism are needed. Here, we report nine unrelated patients with *KCNQ2*-related epilepsy carrying de novo heterozygous *KCNQ2* p.N258K or p.G279D identified via Trio exome sequencing that has never been previously reported. To investigate the molecular mechanisms by electrophysiological techniques combined with immunofluorescence analysis and western blotting. The Cellular localization and protein expression analysis demonstrates that p.N258K and p.G279D impairs surface membrane expression of Kv 7.2. Whole-cell patch-clamp analyses revealed that both variants significantly impaired Kv7.2 M-current amplitude and density, conductance depolarizing shift in voltage dependence of activation, membrane resistance, and membrane time constant (*Tau*), indicating a loss-of-function in both the homotetrameric and heterotetrameric with Kv7.3 channels. In addition, both variants also exerted dominant-negative effects in heterotetrameric with Kv7.3 channels. Thus, novel variants are loss-of-function on Kv7.2 channels, causing infantile-onset epilepsy.

Field of Study: Medical Sciences

Student's Signature

Academic Year: 2022

Advisor's Signature

Co-advisor's Signature

ACKNOWLEDGEMENTS

Firstly, I would like to express my gratitude to my advisor Prof. Vorasuk Shotelersuk and my co-advisor, Assoc.Prof. Saknan Bongsebandhu-phubhakdi for all their guidance, understanding, patience, suggestion and encouragement throughout the time during my studies.

I also would like to express my sincere thanks to all committee member, Prof. Apiwat Mutirangura, Assoc. Prof. Wilai Anomasiri and Assoc. Prof. Thipwimol Tim-Aroon for their helpful suggestion and correction. Most importantly, I would like to give a special thanks to the patients who participated in this study. furthermore, I would like to thank everyone at the Excellence Center for Genomics and Precision Medicine, In particular, Dr. Ponghatai Boonsimma, Dr. Siraprapha Thongkoppet and Dr. Nattarin Jangprasat, who provided assistance, support to laboratory operations and the publication of the journal. Finally, I would like to thank Mrs. Rungnapa Ittiwut and Mr. Phichaya suthivanich for all their supports.

This study was supported by by Health Systems Research Institute (65-040) and National Research Council of Thailand (NRCT); grant number NRCT5-RSA63001-25.

Suphalak Chokvithaya

TABLE OF CONTENTS

	Page
.....	iii
ABSTRACT (THAI).....	iii
.....	iv
ABSTRACT (ENGLISH).....	iv
ACKNOWLEDGEMENTS.....	v
TABLE OF CONTENTS.....	vi
LIST OF TABLES.....	ix
LIST OF FIGURES.....	x
LIST OF ABBREVIATIONS.....	1
CHAPTER I INTRODUCTION.....	2
Background and Rationale.....	2
Research questions.....	3
Objectives.....	3
Hypotheses.....	3
Research design.....	4
Key words.....	4
Ethical consideration.....	4
Expected benefit.....	4
Conceptual framework.....	5
CHAPTER II REVIEW OF RELATED LITERATURE.....	6
Epilepsy.....	6

Next generation sequencing: the diagnostic epilepsy	7
KCNQ2-related infantile-onset epileptic disorders.....	7
The Kv7 potassium channel family.....	9
Highly conservative sequence in Kv7 channel	10
M-currents	11
Overview of mutation in the <i>KCNQ2</i> gene	11
Overview of Electrophysiological method.....	12
Membrane potential, action potential steps.....	15
CHAPTER III MATERIALS AND METHODS.....	17
Patients and clinical data collection	17
Exome, genome sequencing, bioinformatics and variant prioritization.....	17
Generated plasmid constructions	18
KCNQ2 expression in HEK293 cells.....	20
Immunofluorescence	22
Western blotting	23
Fluorescence activated cell sorting (FACS).....	24
Whole cell patch-clamp analysis.....	24
Data analysis	25
CHAPTER IV RESULTS.....	26
Clinical features of the patients.....	27
Molecular characteristics.....	27
Generated plasmid.....	30
1. Generated plasmid constructions; Kv7.2-GFP WT	30
2. Generated plasmid constructions; mutants	32

Fluorescent p.N258K and p.G279D reduces Kv7.2 plasma membrane expression	32
Fluorescence activated cell sorting (FACS).....	34
Electrophysiological properties of p.N258K and p.G279D mutations in Kv7.2.	36
1. Electrophysiological function in the novel p.N258K mutate on of Kv7.2	37
2. Electrophysiological function in the novel p.G279D mutate on of Kv7.2	43
CHAPTER V DISCUSSION	50
APPENDIX.....	53
REFERENCES	60
VITA	68



LIST OF TABLES

	Page
Table 1 Research design of studies.....	4
Table 2 PCR protocol amplified the KCNQ2 gene.....	19
Table 3 TOPO Cloning reaction for generated Kv7.2-GFP plasmid.....	19
Table 4 Mutagenesis protocol for switched amino acid the KCNQ2 gene.....	20
Table 5 Transient transfection protocol.....	21



LIST OF FIGURES

	Page
Figure 1 Conceptual framework of studies.	5
Figure 2 Pathogenic variants associated with the KCNQ2 gene.	8
Figure 3 Structure Kv7 potassium channels.	9
Figure 4 Structure alignment of Kv7 channels and highly conserved sequence on a black background ⁴⁷	10
Figure 5 The structure of single Kv7.2 protein subunit ⁵²	11
Figure 6 Type of patch-clamp configurations.	14
Figure 7 A schematic of neuronal action potential.	16
Figure 8 Setting protocol for whole-cell patch-clamp recording.	25
Figure 9 Sequence alignment of the patient's BAM file on Golden Helix Genome Browse 3.0.0 and pedigree of families.	28
Figure 10 Schemes representation of Kv7 subunits with different mutation locations in Kv7.2 subunits.	29
Figure 11 Polymerase chain reaction (PCR) of the KCNQ2 gene.	30
Figure 12 Plasmid constructions; Kv7.2-GFP WT.	31
Figure 13 Chromatograms of sanger sequencing verified quality of the mutations.	32
Figure 14 Immunofluorescence confocal microscopy showed localization on cell membranes. ...	33
Figure 15 Western blots of Kv7.2 protein expressions in membrane, cytoplasmic and total cell lysate.	34
Figure 16 Histogram profiles of sorting gates used for FACS based on Alexa Fluor 430 and 647 channels.	35

Figure 17 Representative raw current traces for homotetrameric and heterotetrameric in p.N258K channels.....	38
Figure 18 Comparison of average peak M-current densities (pA/pF) at +50 mV in homotetrameric and heterotetrameric of p.N258K channels.	39
Figure 19 Analysis of the current–voltage (I-V) relationships (from -110 to +50 mV) and comparison of reversal potential in homotetrameric and heterotetrameric of p.N258K channels.	40
Figure 20 Comparison of K ⁺ gating properties in homotetrameric and heterotetrameric p.N258K channels.....	41
Figure 21 Comparison of the membrane resistance (R _m) and the membrane time constant (Tau) in homotetrameric and heterotetrameric of p.N258K channels.	42
Figure 22 Representative raw current traces for homotetrameric and heterotetrameric in p.G279D channels.....	44
Figure 23 Comparison of average peak M-current densities (pA/pF) in homotetrameric and heterotetrameric of p.G279D channels.	45
Figure 24 Analysis of the current–voltage (I-V) relationships (from -110 to +50 mV) and comparison of reversal potential in homotetrameric and heterotetrameric of p.G279D channels.	46
Figure 25 Comparison of K ⁺ gating properties in homotetrameric and heterotetrameric p.G279D channels.....	47
Figure 26 Comparison of the membrane resistance (R _m) and the membrane time constant (Tau) in homotetrameric and heterotetrameric of p.G279D channels.	48

LIST OF ABBREVIATIONS

BFNC	Benign familial neonatal convulsion
DEE	Developmental and epileptic encephalopathy
KCNQ2	Potassium voltage-gated channel subfamily Q member 2
KCNQ3	Potassium voltage-gated channel subfamily Q member 3
Kv7	Voltage-gated potassium channels number 7

AMINO ACID

A	Alanine (Ala)	N	Asparagine (Asn)
C	Cysteine (Cys)	P	Proline (Pro)
D	Aspartate (Asp)	Q	Glutamine (Gln)
E	Glutamate (Glu)	R	Arginine (Arg)
F	Phenylalanine (Phe)	S	Serine (Ser)
G	Glycine (Gly)	T	Threonine (Thr)
H	Histidine (His)	U	Selenocysteine (Sec)
I	Isoleucine (Ile)	V	Valine (Val)
K	Lysine (Lys)	W	Tryptophan (Trp)
L	Leucine (Leu)	Y	Tyrosine (Tyr)
M	Methionine (Met)		

CHAPTER I INTRODUCTION

Background and Rationale

Infantile-onset epilepsy represents one of the most challenging pediatric neurological conditions to diagnose and manage. It occurs in 0.8-1.2 per 1000 live births¹⁻³ and over 300 genes have been demonstrated to be involved in the pathogenesis of infantile-onset epilepsy⁴. Among these genes, *KCNQ2*, encoding the potassium channel subunit, have been implicated to cause benign/self-limited neonatal seizures (MIM#121200) or developmental and epileptic encephalopathy (DEE; MIM#613720)⁵, in which de novo *KCNQ2* mutations underlie a substantial proportion of patients. In general, patients with *KCNQ2* mutations have seizures that occur during the first week of life whereas in benign/self-limited neonatal seizures patients show seizures in the first days after birth and the seizures stops after weeks to months^{6,7}. The developmental trajectory is typically within normal range. DEE phenotype characterized by drug-resistant epilepsy and significant developmental delay⁸⁻¹⁰. Electroencephalogram (EEG) typically shows suppression-burst pattern. Identifying causative mutations and its phenotypes is critical for genetic counseling and patient management.

The *KCNQ2* gene encodes Kv7.2 protein subunits that assemble the tetrameric homomer voltage-gated potassium channels (Kv7.2 channels). On the other hand, heterotetrameric channels (Kv7.2/Kv7.3) co-express with Kv7.3, encoded by the *KCNQ3* gene. Each subunit of Kv7.2 protein consists of intracellular amino (N) and carboxy (C) terminals, six transmembrane segments (S1–S6), and a pore loop between S5 and S6. Transmembrane segments between S1 and S4 forms a voltage sensing domain (VSD). The N-terminus (-NH) is tetramerization domain that determines the specificity of subunit assembly¹¹⁻¹³. Kv7.2/Kv7.3 channels are mainly located in the soma and axon of neuron while Kv7.2 is expressed in axon terminals of neuron¹⁴. Both channels underlie the M-current, a slowly excitation current, non-inactivating current, a subthreshold voltage-gated potassium current that regulates neuronal excitability and is inhibit by muscarinic receptor agonists. M-current is typically produced by heterotetrameric tetramerize while the homotetrameric Kv7.2 or Kv7.3 ion channel produces a small M-current¹⁵.

To date, at least one hundred ninety-four cases of KCNQ2-related epilepsy have been reported with mutations distributed over the six transmembrane, either at different domains or within the same location but with different amino acids leading to varying severity^{16,17}. Therefore, the functional study of the Kv7.2 channels lead to a better understanding of the pathogenesis. Studying the pathogenic mutations in the KCNQ2 gene provides a better understanding of the molecular pathomechanism of the disease and can be used as a guideline for treatments. Here, we report the clinical characteristics of nine patients with neonatal-onset seizures with KCNQ2 mutations. Two variants have never been previously reported. We perform study to investigate the electrophysiological functional effect of both variants and found that they are both loss-of-function which suggest specific treatment.

Research questions

What are functionally consequences of variants?

Objectives

To determine the functional consequences of the newly identified p.N258K and p.G279D variants the pore loop domain of Kv7.2 channels by electrophysiological analysis, immunofluorescence and western blotting in transfected HEK293 cells.

Hypotheses

Variants are loss of function on Kv7.2 channels, causing infantile-onset epilepsy.

Research design: descriptive and in vitro studies

Table 1 Research design of studies.

Experimental	Objective
1. Molecular biology	Generation plasmid wild types and mutant Kv7.2 subunits
2. Cell culture and transfections	Plasmid transfer allows the study of gene function and protein expression in the cellular environment.
3. Immunofluorescence	Confirm mutant proteins localization into surface membrane
4. Western blotting	Confirm mutant proteins expression
3. Fluorescence activated cell sorting (FACS)	Identification expressed cells after transfection
4. Electrophysiology (Whole-cell patch technique)	Functional analysis of voltage-gated potassium channel

Key words

Developmental and epileptic encephalopathy (DEE); Self-limited neonatal seizures; The KCNQ2 gene; whole-cell patch-clamp analysis.

Ethical consideration

Ethical approval of the study protocol had been provided by the Institutional Review Board of the Faculty of Medicine, Chulalongkorn University, Bangkok, Thailand (IRB No. 452/64) and the study followed the Helsinki Declaration and Good Clinical Practice guidelines.

Expected benefit

An implication of the finding is critical for precision medicine.

Conceptual framework

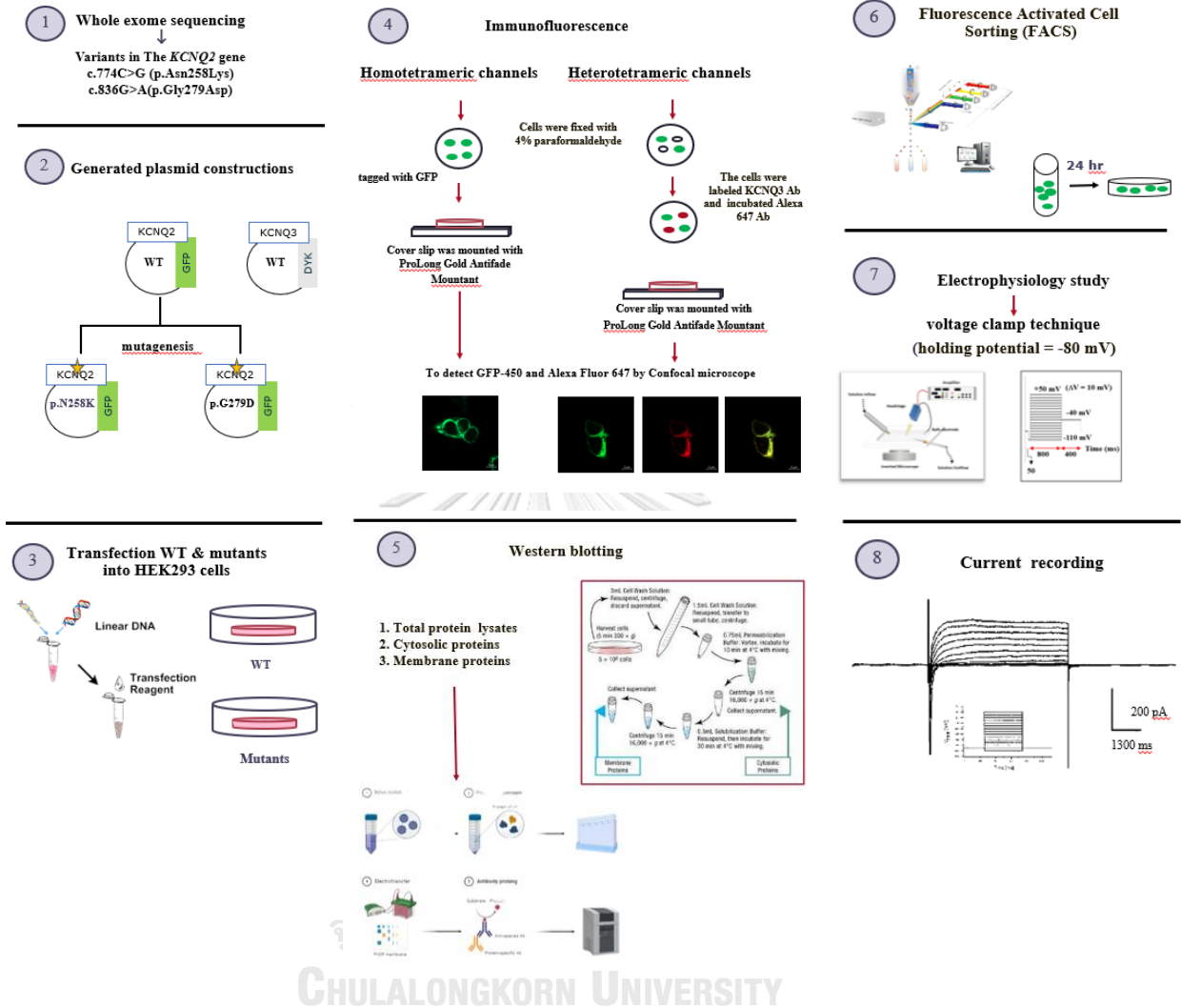


Figure 1 Conceptual framework of studies.

CHAPTER II REVIEW OF RELATED LITERATURE

Epilepsy

Epilepsy is one of the most common chronic neurological diseases. It occurs in 0.8-1.2 per 1000 live births and nearly 25% is pediatric epilepsy^{18,19}. Epilepsy have been identified by the recurrence of unstimulated seizures. According to the International League Against Epilepsy (ILAE) have defined epilepsy based on recurrent the following conditions: (1) At least two unprovoked (or reflex) seizures occurring >24 h apart; (2) one unprovoked (or reflex) seizure and a probability of further seizures similar to the general recurrence risk (at least 60%) after two unprovoked seizures, occurring over the next 10 years; (3) two or more unprovoked seizures occurring at least 24 h apart that diagnosed of an epilepsy syndrome^{18,20,21}. In addition, about 10.5 million children (< 15 years old) have epilepsy. Most children with epilepsy have been divided into four prognostic group. The first group is benign epilepsy (self-limiting; 20-30% of patients) which have been resolved spontaneously in a few years and often avoids treatment, such as Benign infantile seizures (non-familial) and Benign familial neonatal convulsions (BFNC). The second group is drug-sensitive epilepsy (30% of patients), in which seizures are controlled with medication and spontaneous relief is achieved within a few years. The third group is drug-dependent epilepsy which drug treatment have been control seizures but no spontaneous respite (20% of patients), required lifelong drug therapy, such as juvenile myoclonic epilepsy. The fourth group is drug-resistant epilepsy with a poor prognosis (13–17 % of patients), such as epileptic encephalopathy (EE)²². The clinical spectrum of epilepsy varies from patient to patient. Thus, treatment in patients have different antiepileptic therapy. For example, antiepileptic therapy retigabine (potassium channel opener) or dalfampridine (potassium channel blocker)^{23,24}.

Epilepsy occurs for many reasons, such as genetic mutations, brain disorder, metabolic diseases, injuries and neurological infections. A variety of genes have been associated with epilepsy. there suggests that several gene functions involve in disease progression. However, often genetic differences or phenotype differences makes diagnostic methods very difficult. Currently, next generation sequencing (NGS) allows the discovery of many genes that cause disease in humans²⁵. Consequently, NGS is widely used in the genetic diagnosis of epilepsies²⁶.

Next generation sequencing: the diagnostic epilepsy

In 1977, the primary DNA sequencing method was introduced by Sanger, Maxam and Gilbert²⁷. This sequencing has been developed and read base sequences up to 2 kilo base pairs (Kbps). Longer DNA fragments sequencing was developed by during the Human Genome Project²⁸. In 2004, Next Generation Sequencing (NGS) is a large parallel sequencing platform. The DNA templates are randomly read based on the genome. NGS offers multiple platforms, such as the 454 pyrosequencing, illumination sequence. All are based on the same procedure. First, the DNA templates are randomly split into fragments. Then, the fragments are conjugated with an adapter specific to the primer used for amplification. After that, clonal expansion, each one with the same template is sequenced. Every cycle of adding probes or nucleotides show an observable signal to the image. The number of read lengths with NGS is 50-500 base pairs. Lastly, NGS reads are aligned to the reference sequence²⁹. These NGS technologies are now used in a wide variety of contexts. Neurogenetics services was supported by Whole Exome Sequencing (WES) for identification novel variants in the genes, such as *CHD2*, *COL4A1*, *FOXP1*, *GABRA1*, *GRIN2B*, *HNRNPU*, *KCNQ2*, *MECP2*, *PCDH19*, *SCN1A*, *SCN2A*, *SCN8A*, *SLC6A1*, *STXBPI* and *WWOX* gene³⁰.

KCNQ2-related infantile-onset epileptic disorders

Mutations in the *KCNQ2* gene contribute to neonatal epilepsy with significant phenotype heterogeneity, ranging from mild of the spectrum, like benign familial neonatal seizures (BFNS) to more severe of neonatal onset developmental and epileptic encephalopathy (DEE). In addition, *KCNQ2*-DEE have been shown approximately 25–30% prevalence in individuals with autism spectrum disorder (ASD)^{31,32}. *KCNQ2*-BFNS is characterized by multifocal seizures starting in first day of life. There is usually a normal pattern in the electroencephalogram (EEG). Seizures usually occur for a short time (one to two minutes) on any part of the body or in general. Most children epilepsy remits spontaneously after few weeks or months (self-limited seizures)³³. In contrast, *KCNQ2*-DEE (also classified neonatal encephalitis type 7 or DIEE-7) is often a de novo *KCNQ2* mutation and is characterized by multiple daily drug-resistant seizures. It begins in the first week of life and ends between the ages of 1-4 years. The EEG presents burst suppression pattern. Generally, it has a very poor development and prognosis^{32,34,35}.

In previous studies, pathogenic variants associated with KCNQ2-related self-limited neonatal seizures are truncating variants (splice, nonsense, and frameshift), whole-gene deletions, or heterozygous missense variants resulting in haploinsufficiency with a 20%-30% reduction of the M-current density when mutated subunits are expressed together with wild type subunits in heterologous cell systems^{5,36}. Several previous studies analyzed the effect KCNQ2-related self-limited neonatal seizures mutations have on the electrophysiological properties of K⁺ channels³⁷⁻³⁹. Most mutations reduced the M-current density by about 20–30%, causing haploinsufficiency of the ion channel. Only three KCNQ2 mutation with a dominant negative effect had been published reduction in M-current density by more than 50%. The p.N258S mutation in S5-H5 linker reduced M-current density by more than 50% (~50-60%)⁴⁰. The p.R207W mutation in S4 segments did not lead to KCNQ2-related self-limited neonatal seizures alone, but also caused myokymia in the same patient. That is able to reduce M-current density by more than 50% while the p.S247W mutation in S5 segments led to BFNC. that is able to reduce M-current density by more than 80%^{41,42}. Pathogenic changes identified in KCNQ2-related developmental and epileptic encephalopathy are all de novo heterozygous missense variants or in-frame indels shown to exert more than 50% reduction of the M-current function^{43,44}. Variants associated with KCNQ2-NEO-DEE are clustered in the S4 voltage-sensor, the pore, the C-terminal proximal segment, and near the C-terminal B helix; all these regions are critical determinants for channel function⁵.

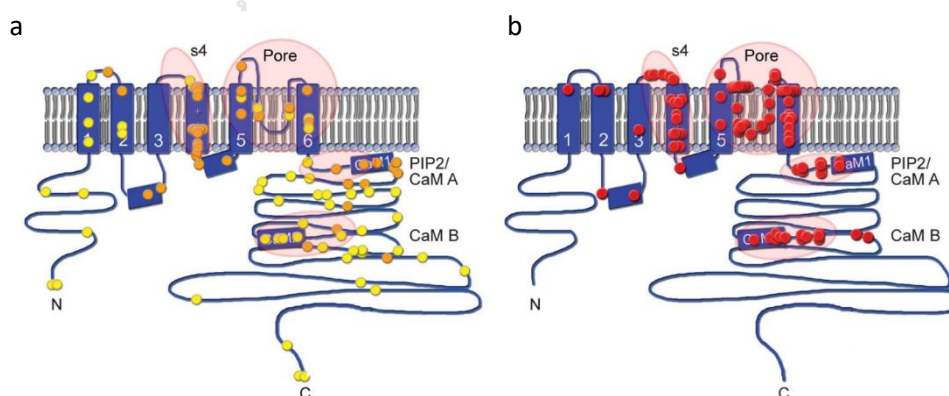


Figure 2 Pathogenic variants associated with the *KCNQ2* gene.

(a) Mutations found in BFNE/BFNIS/BFIS cases are distributed among all areas of Kv7.2 protein subunit. (b) Mutations found in epileptic encephalopathy are nearly the 4 hot spots: the S4 voltage-sensor, the pore, the proximal C-terminal domain that binds phosphatidylinositol 4,5-bisphosphate (PIP2) and calmodulin¹⁷.

The Kv7 potassium channel family

Kv7 (KCNQ) family channels represent voltage-gated potassium (K⁺) channels which consist of five members (Kv7.1-7.5) is generated by the KCNQ gene family. KCNQ1-5 gene are located at chromosome 11p15, 20q13.3, 8q24, 1p34 and 6p14¹¹. Similarly, to other potassium channels, a usable Kv7 channel produces identical or compatible subunit tetramers. Each subunit consists of six transmembrane segments (S1–S6), amino (-NH) and carboxylic (-COOH) terminal. Transmembrane segments between S1 and S4 forms a particular voltage sensing domain (VSD). The S4 is important to the channel as it requires four to six positively charged arginine for voltage sensing to function properly. The pore-loop domain, the selectivity filter, is formed by S5–S6 segment; within this region, there must be a conserved GYG motif as a sequence of K⁺ permeability control^{45,46}. Long intracellular C-terminus where is four regions of α -helix (A–D) that involved in signal capture and transduction activities by critical regulators, such as phosphatidylinositol 4,5-bisphosphate (PIP2), calmodulin (CaM), syntaxin, A-kinase-anchoring proteins, protein kinase C and ankyrin-G⁴⁷. The N-terminus is tetramerization domain that determines the specificity of subunit assembly (Fig. 3)⁴⁵. The *KCNQ1* gene forms homomeric channels relate to cardiac action potential. The *KCNQ2-5* gene, the neuronal isoforms of the channels that are regulate neurotransmitter release⁴⁸.

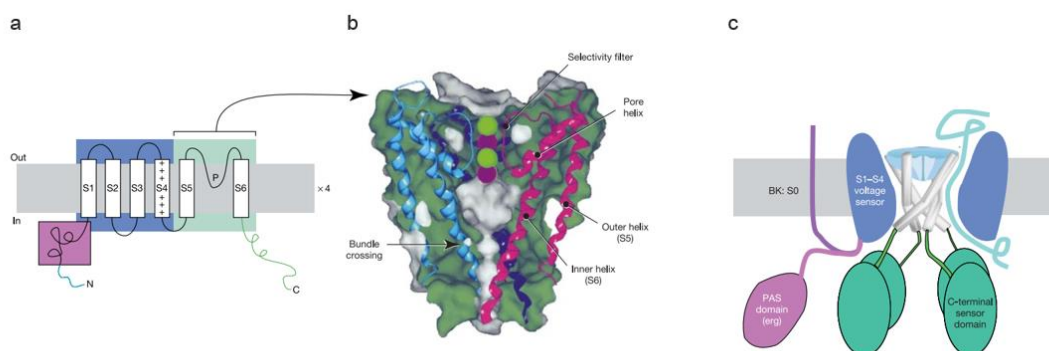


Figure 3 Structure Kv7 potassium channels.

(a) Kv7 proteins subunit (six transmembrane protein) (b) the selectivity filter. (c) Kv7 potassium tetrameric channels⁴⁵.

Highly conservative sequence in Kv7 channel

Kv7 channels have highly conservative sequence⁴⁹. First of all, S4 segment is R-F-L-Q-I-L-R-M, which is an important and regional voltage detector sequence. It must be four to six positively charged arginine. Second, the S5-P-S6 is T-I-G-Y-G-D-K which is selectivity filter, specifically G-Y-G motif that is signature sequence for filter ion (Fig. 4)^{50,51}. Lastly, α -helices A-B in carboxylic tail is D-V-I-E-Q-Y-S as specific interaction with CaM (Fig. 4)⁴⁷.

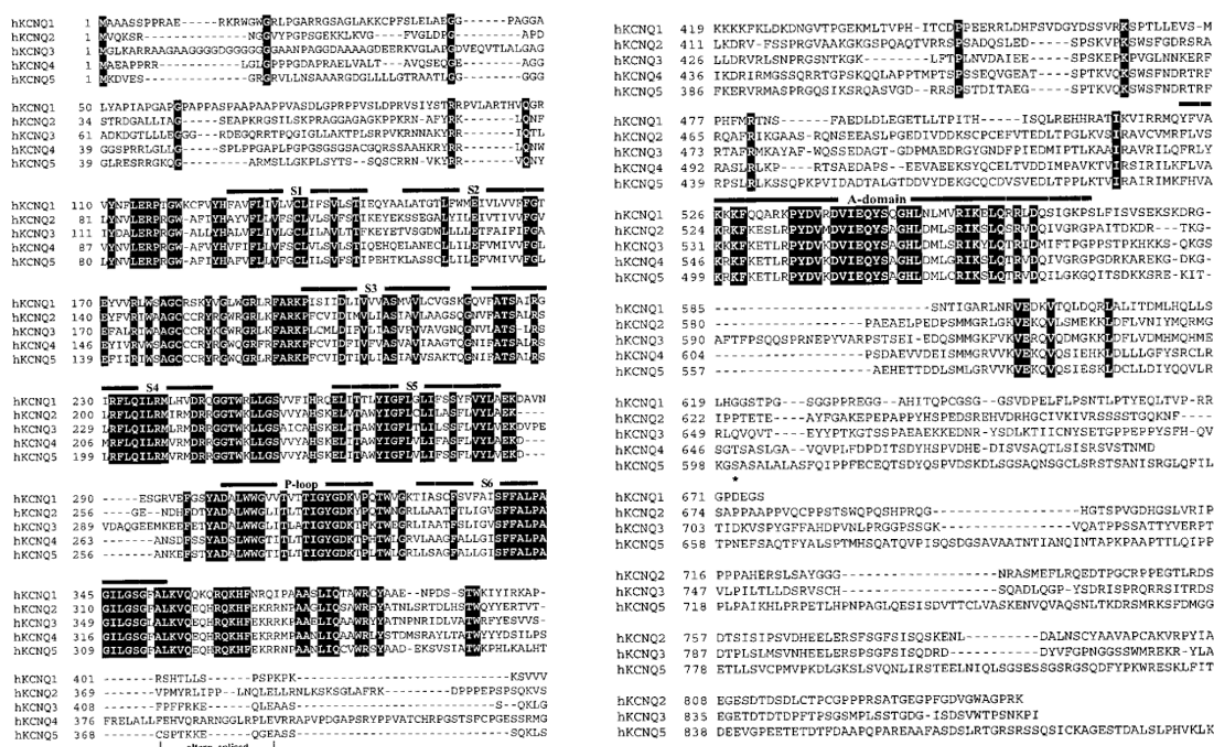


Figure 4 Structure alignment of Kv7 channels and highly conserved sequence on a black background⁴⁷.

The *KCNQ2* gene encodes Kv7.2 protein subunit that assemble the tetrameric K⁺ channels (Kv7.2 channels). On the other hand, heteromeric channels (Kv7.2/Kv7.3) co-expressed with Kv7.3, encoded by the *KCNQ3* gene. Kv7.2/Kv7.3 channels are mainly expressed in the central nervous system (Soma & Axon) while Kv7.2 expressed of the peripheral nervous system¹⁴. Both of channels produced the M-current, slowly excitation current, non-inactivating current, a subthreshold voltage-gated potassium current which control neuronal excitability and is inhibited by

muscarinic receptor agonists. Typically, wild-type M-current is produced by heteromeric tetramerize while homomeric KCNQ2 or KCNQ3 ion channels produce small M-currents.

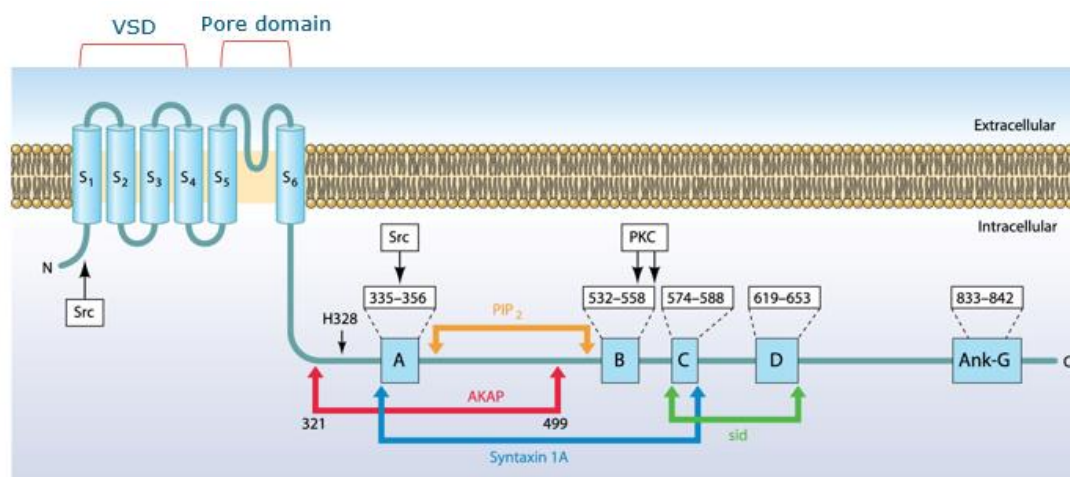


Figure 5 The structure of single Kv7.2 protein subunit⁵².

M-currents

The M-current is a type of non-stimulating potassium current (Kv7/KCNQ family) which is important in raising the threshold for firing an action potential. It turns on at rest and tends to open more during depolarization. Additionally, when the muscarinic acetylcholine receptor (MACHR) is activated, the channel is closed. The M-channel is a PIP₂-regulated ion channel^{15,53}.

The role of M currents in KCNQ2-pathogenic variants lead to the spectrum of neurodevelopmental disorders. Pathogenic variants associated with KCNQ2-BFNS that were splice, nonsense, frameshift, gene deletion, and heterozygous missense variant. There resulted in a 20-30% reduction in M- current density when mutated subunits were expressed in the heteromeric channels. On the other hand, KCNQ2-DEE is caused by heterozygous de novo missense and have been shown a dominant negative (>50% decrease in M-current density) or gain of function (GOF; >100% of the M-current density) in the heteromeric channel³⁶.

Overview of mutation in the *KCNQ2* gene

The mutation hotspots of KCNQ2-pathogenic are found in S4 segment, the pore region and the intracellular C- terminal domain. These mutations have been consisted of 95%missense

mutations, 13% frameshift mutations, 9% splice site, 5% nonsense mutations. Currently, more than one hundred have been reported data¹⁶. In a previous functional study, the p.R213Q and p.R213W mutations in S4 segment have been showed a markedly reduce sensitivity to voltage⁴³. Mutation studies in the pore domain, p.A265P, p.T274M, p.G290D are of loss of function which have been reduced the M-current amplitude associated with the EE⁴⁴. One study in Kv7.2-EE, p.R325G mutation in C-terminus reduced channel apparent affinity for PIP2 which made non-functional⁵⁴. Additionally, the p.M1V, this variant is an initiation codon that leads to abnormal protein translation⁵⁵.

Overview of Electrophysiological method

Electrophysiology is the branch of electrical physiology that is the measurement of the electrical activity of biological cells (muscle cells, neurons, or stem cells). This can be done at a single cell level or measured simultaneously from hundreds or thousands of cells⁵⁶.

Electrophysiological techniques are divided into two types.

1. Intracellular recording

1.1 Patch-clamp: It involves creating a series circuit that contains cells or membranes without penetrating the cell wall. An ionic solution-filled glass micro-pipette attached to the clamp amplifier creates a high-resistance (Giga-ohm = $G\Omega$) seal between the patch and the glass in the pipette mouth⁵⁷.

1.2 Current-clamp: Cells is injected the known current amplitude, such as increasing step current from -50 to +50 pA ($\Delta = 10$ pA) observed the change in cellular excitability in response to these current injections. It is a valuable technique because it can mimic physiological situations such as synaptic input⁵⁷.

1.3 Voltage-clamp: The membrane potential is held at the rated voltage. Ion channels open at various command voltages. This means that the resistance of the membrane changes when an ionic current flows through the membrane. The feedback amplifier instantly compensates for this by injecting feedback current to maintain the cell at the command voltage and record the resulting current⁵⁸.

(2) Extracellular recording: This technique involves placing a wire electrode or silicon probe directly into an object, in vivo, primary cell stratification and cultured cells or a biopsy above the electrode in vitro⁵⁹.

Patch-clamp is a conventional technique of electrophysiology. It requires an initial formation of a Giga-ohm ($G\Omega$) seal between the plasma membrane and the blunt tip (0.5–1 μm diameter) of glass micropipette (electrode). The Giga-ohm seal maintains the integrity of the plasma membrane (unbreakable) and prevents the solution inside the micropipette from entering the cell. However, this also limited electrical access to the intracellular spaces. This resulted in the inability to control the cell membrane potential. Therefore, the perforation technique is a strong suction or short momentary pressure after the formation of a Giga-ohm seal to rupture the intact plasma membrane. then, glass micropipette was used measuring ion flow through ion channels or across cell membrane. Patch-clamp configurations have four basic techniques. (1) cell-attached patch records current through single, or a few, ion channels contained in the patch of membrane (no rupture membrane). It requires a high resistance (10-100 $G\Omega$) seal between the electrode and the membrane. (Fig. 6A). (2) Whole-cell patch records current through multiple channels. The cells is confined to the resting membrane potential (-70 to -80 mV) and negative pressure is applied to rupture the membrane. It requires 2- 6 $G\Omega$ resistance (Fig. 6B). (3) Outside-out patch records current through single channel. Membrane is slowly drawn from the cell, allowing a bubble of membrane out from the cells (Figure 6C). (4) Inside-out patch records current through single channel from that its membrane have been detached at the cytosolic surface in low Ca^+ solution (Fig. 6D)⁶⁰.

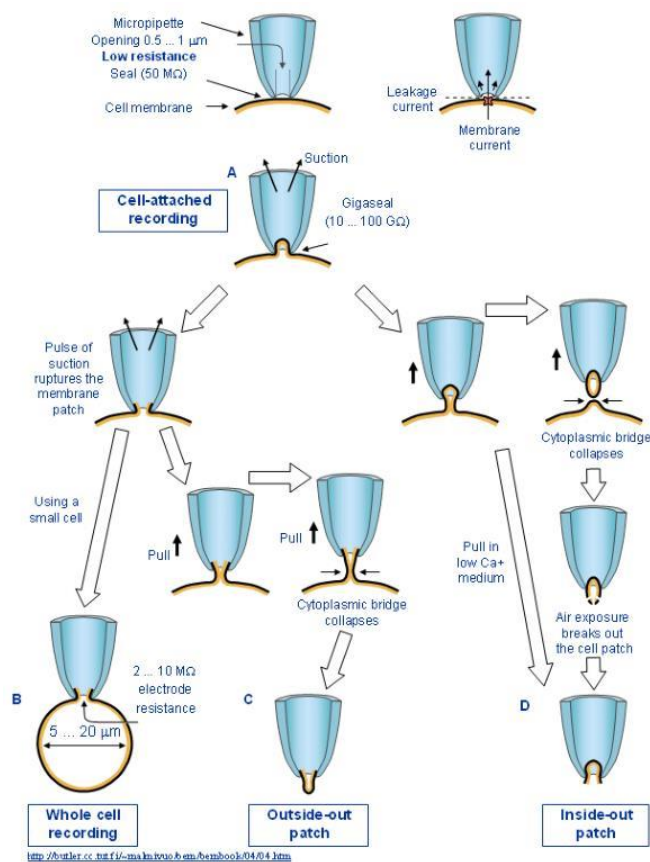


Figure 6 Type of patch-clamp configurations.

(A) Cell-attached patch (B) Whole-cell patch (C) Outside-out patch (D) Inside-out patch.

In this study, whole-cell patch was used to study ion channel function. this technique makes intracellular recording very stable. But the disadvantage is that the intracellular fluid of the cell mixes with the solution inside the electrode. In addition, command voltages are important in the study of ion channel functions because ion channels are open at different command voltages that lead to the resistance of the membrane to change when an ionic current flows through the membrane. Therefore, understanding the membrane potential phase and its operation is very important in determining the voltage phase in this study.

Membrane potential, action potential steps

Membrane potential is the potential difference between cell membranes. The potential difference is due to the charges separated from the hydrophobic membrane which acts as both a capacitor and a resistance to the movement of charged ions. Most of the ions in cells are Na^+ , K^+ , Ca^{2+} and Cl^- . These ions have different concentrations inside and outside the cell. So, when the ion channel opens, the ions move to balance the ion concentration. In general, Na^+ , Ca^{2+} and Cl^- ions are more concentrated outside the cell and K^+ ions are more concentrated than inside the cell, in which the cell has a negative charge. This sets up an electrochemical gradient as the ion channels open. The permeable ions flow down their electrochemical charge gradient through the membrane and cause a change in voltage. This results in either depolarization or hyperpolarization of the cell membrane potential. The positively charged Na^+ and Ca^{2+} ions had an electrochemical gradient that supports their movement towards negatively charged cells, so their positive charge depolarizes. On the other hand, K^+ ions are highly concentrated inside the cell. Therefore, the driving force of the ions is in the opposite direction, away from the cell. As a result, they take the positive charge out of the cell and make the cell membrane more negative. This is called hyperpolarization. The flow of ions through the membrane determines the total resistance. (According to Ohm's law; $V = IR$) if there are many of channels open, membrane resistance (R_m) is less due to more openings. Another important property of membranes is capacitance (C_m). Cells with high capacity and low conductance change the potential slowly while cells with less capacity change quickly. The velocity of this change is the membrane time constant ($R_m \times C_m = \text{Tau}$). In action potential of neurons, resting membrane potential (around -60 mV) have been activated by a synaptic input. The depolarization reaches "threshold" this triggers the opening of Na^+ channels (-55 mV). This causes a rapid influx of Na^+ ions leading to the rise membrane potential at +40 mV. After that, Na^+ channels are quickly inactivated while K^+ channels is activate. This efflux of K^+ ions repolarize the membrane back to -60 mV or beyond to more negative potentials, causing an after hyperpolarizing potential. hyperpolarization uses slowly times, a small concentration of the ions exchanged across the membrane are pumped back by Na^+/K^+ pumps that exchange K^+ and Na^+ ions to reset and maintain the resting potential (Fig. 7) ⁶¹.

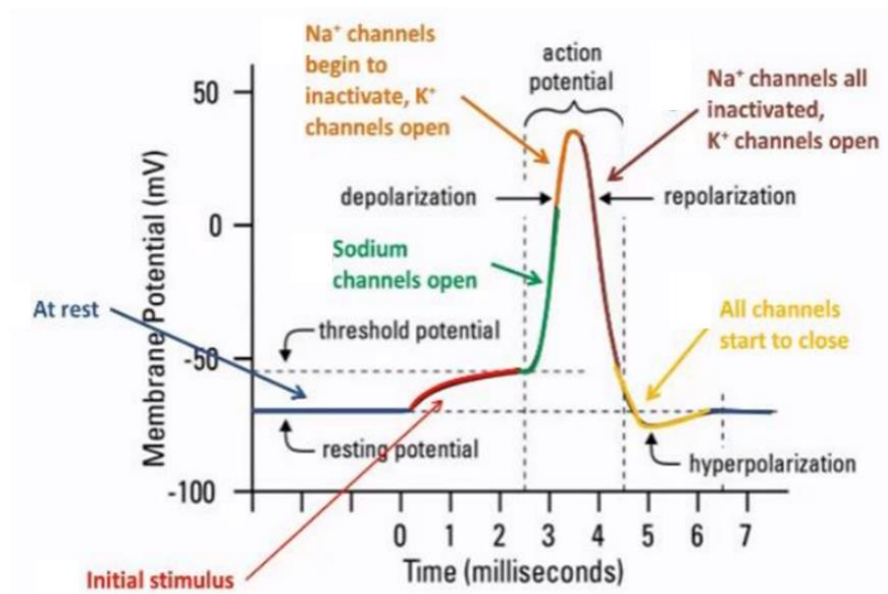


Figure 7 A schematic of neuronal action potential.



CHAPTER III MATERIALS AND METHODS

Patients and clinical data collection

Ethical approval was obtained from the institutional review board of the Faculty of Medicine, Chulalongkorn University. Written informed consents were obtained from parents or legal guardians of the participants. From June 2016 to December 2020, we recruited 104 patients with infantile-onset pharmacoresistant epilepsy, defined as failure of adequate trials of two tolerated, appropriately chosen, and used antiepileptic drugs,⁶² who underwent exome and/or genome sequencing at King Chulalongkorn Memorial Hospital. Nine patients were found to harbor pathogenic or likely pathogenic variants in the *KCNQ2* gene. The detailed demographic data and clinical characteristics were collected.

Exome, genome sequencing, bioinformatics and variant prioritization

Genomic DNA was isolated from peripheral blood leucocytes, enriched by SureSelect Human All Exon V5 kits (Agilent Technologies, Santa Clara, CA) and sent to MacroGen Inc., Seoul, Korea for exome sequencing or to Beijing Genomics Institute (BGI), Beijing, China for genome sequencing. Illumina HiSeq 2000 Sequencer was used with a target output of 6 GB. Sequence reads in FASTQ sequencing files were aligned to the Human Reference Genome hg19 from UCSC using Burrows-Wheeler Alignment (BWA) software (<http://bio-bwa.sourceforge.net/>). Single nucleotide variants (SNVs) and small insertions/ deletions (indels) were detected by GATK Haplotypecaller and annotated by dbSNP&1000G.

A list of 728 genes associated with Genetic Epilepsy Syndrome according to Genomics England PanelApp (<https://panelapp.genomicsengland.co.uk/panels/402/>) were used for the first step of analysis. In silico analysis including SIFT (<http://sift.jcvi.org/>); Polyphen-2, (<http://genetics.bwh.harvard.edu/pph2/>); M-CAP (<http://bejerano.stanford.edu/mcap/>); CADD (<https://cadd.gs.washington.edu/>; recommended pathogenicity threshold >20) were also used to predict variants' pathogenicity. Variants were considered novel if they were not previously reported in Genome Aggregation Database (gnomAD), ClinVar (<https://www.ncbi.nlm.nih.gov/clinvar/>), not documented in PubMed scientific literature, and were not identified in our in-house Thai reference exome database (T-REx)⁶³. Variants were

classified according to the recommendation of American College of Medical Genetics and Genomics (ACMG)⁶⁴.

Generated plasmid constructions

pcDNA3.1+/KV7.2-DYK (#NM_004518.6) and pcDNA3.1+/KV7.3-DYK (#NM_004519.4) were synthesized by Genscript (New Jersey, USA). The cDNA_{KV7.2} was then subcloned into the pcDNA3.1/CT-GFP-TOPO Vector (Invitrogen, Massachusetts, USA) using standard PCR techniques (Table 2,3). Point mutations, c.774C>G (p.Asn258Lys) and c.836G>A (p.Gly279Asp), were introduced using QuickChange site-directed mutagenesis kit (Agilent Technologies, Santa Clara, California, USA). Mutagenic primers (Table 4) for each variant were designed using the QuikChange Primer Design website (<https://www.agilent.com/store/primerDesignProgram.jsp>). All plasmids were verified quality using Sanger sequencing.

PCR protocol

1. To prepare master mix for one reaction (plus one extra) and add template plasmid,
2. Gently vortex and samples and spin down.
3. Perform PCR reaction using thermal cycling condition

Table 2 PCR protocol amplified the *KCNQ2* gene.

(a) Primer used for amplification sequences of the *KCNQ2* gene. (b) Reaction mix (c) Thermal cycling conditions

a

Fragment	Forward Primer (5'-3')	Reverse Primer (5'-3')	PCR size (bp.)
<i>KCNQ2</i> gene	AAAAGCTTCCAGGCACCATGGTGCAG	TCTTCCTGGGCCCGGCCAG	2,577

b

Ingredients	Volume (μ L)
MgCl ₂ (25mM)	1.8
10X PCR buffer+ (NH ₄) ₂ SO ₄	2
dNTP (10mM)	0.3
Forward primer (10 μ m)	0.3
Reverse primer (10 μ m)	0.3
<i>Taq</i> DNA polymerase (5u/ μ l)	0.12
DMSO 5%	1
dH ₂ O	13.18
DNA (50ng/ μ l)	1
Total	20

c

Step	Temperature ($^{\circ}$ C)	Time	Number of cycles
Initial denaturation	94	5 min	1
Denaturation	94	30 s	
Annealing	62	30 s	35
Extension	72	2.30 min	
Final Extension	72	10 min	1

Cloning the *KCNQ2* gene into pcDNA3.1/CT-GFP_TOPO

1. Warm Super Optimal Broth (SOC) medium and Lysogeny broth (LB) plates at room temperature.
2. Set up TOPO Cloning reaction

Table 3 TOPO Cloning reaction for generated Kv7.2-GFP plasmid

Ingredients	Volume (μ L)
Fresh <i>KCNQ2</i> product	4
Salt Solution	1
TOPO vector	2
Total	6

3. Mix reaction and incubate for 30 minutes at room temperature.

Transformation

1. Thaw on ice of TOP10 Competent *E.coli* 50 μ L
2. Add 2 μ L of TOPO Cloning reaction into TOP10 Competent *E.coli* and mix gently and Incubate on ice 30 minutes

3. Heat-shock the cell for 30 seconds at 42 °C and add 950 μ L of SOC medium
4. Shake the tube horizontally (200 rpm) at 37 °C for 1 hour.
5. Spread 100 μ L of pellet into LB plates and incubate overnight at 37 °C
6. Pick colony for analyze the *KCNQ2* gene by PCR and verify the orientation of insert by restriction enzyme (HindIII and EcoRV)
7. The *KCNQ2* gene verified quality using Sanger sequencing

Mutagenesis protocol

1. To prepare each mutagenesis reaction
2. Gently vortex and samples and spin down.
3. Perform PCR reaction using thermal cycling conditions

Table 4 Mutagenesis protocol for switched amino acid the *KCNQ2* gene.

(a) Primer used for amplification sequences. (b) Reaction mix (c) Thermal cycling condition

a

Fragment	Forward Primer (5'-3')	Reverse Primer (5'-3')
c.774C>G (p.N258K)	GAAGGGGAGAAGGACCACTTTGACACCTA	TAGGTGTCAAAGTGGTCCTTCTCCCCCTTC
c.836G>A (p.G279D)	TGACCACCATTGACTACGGGGACAAGTACC	GGTACTTGTCCCCGTAGTCAATGGTGGTCA

b

Ingredients	Concentration	Volume (μ L)
10X reaction buffer		5
dNTP (10mM)		1
Forward primer (125 ng/ μ l)	100 ng/ μ l	1.25
Reverse primer (125 ng/ μ l)	100 ng/ μ l	1.25
dH ₂ O		16
DNA (50ng/ μ l)		0.5
Total Master Mix		25
Add Pfu Ultra DNA polymerase	5u/ μ l	1

c

Step	Temperature (°C)	Time	Number of cycles
Initial denaturation	94	30 s	1
Denaturation	95	30 s	
Annealing	55	1 min	15
Extension	68	9 min	
Final Extension	68	1 min	1

KCNQ2 expression in HEK293 cells

To begin with, HEK293 (human embryonic kidney; ATCC CRL-1573) cells, native non-expression the *KCNQ2* and *KCNQ3* genes, using in this study were passage 7–15. Then, cells were cultured in Dulbecco's Modified Eagle Medium (DMEM) with high glucose (HyClone, Logan, Utah, USA), supplemented with 10% Fetal bovine serum and 1X Antibiotic-Antimycotic (Gibco) and maintained at 37 °C in a humidified atmosphere with 5% CO₂. Next, plasmids were

transient transfected into HEK293 cells using Lipofectamine 3000 (Invitrogen) according to protocol in Table 5. For the homotetrameric (Kv7.2, p.N258K, p.G279D) with 2.5 μg , or heterotetrameric (Kv7.2/Kv7.3, p.N258K/Kv7.3, p.G279D/Kv7.3, Kv7.2/p.N258K/Kv7.3, Kv7.2/p.G279D/Kv7.3) were co-expressed by transfecting in a 1:1 ratio (1.25 μg : 1.25 μg), 1:1:2 ratio (0.625 μg : 0.625 μg : 1.25 μg) and assayed 48- or 72- hours post transfection.



Table 5 Transient transfection protocol.

For (a) Whole cell patch-clamp analysis (b) Immunofluorescence (c) Western blotting

a Whole cell patch-clamp analysis (6-well)

Condition	Cells	Working Lipofectamine 3000 Reagent			DNA Master mix	
		Lipofectamin3000 (uL)	Opti_MEM (uL)	Plasmids (ng)	P3000 (uL)	Opti_MEM (uL)
p.Kv7.2	1,000k	7.5	125	2500	5	125
p.Kv7.3	1,000k	7.5	125	2500	5	125
p.N258K	1,000k	7.5	125	2500	5	125
p.G279D	1,000k	7.5	125	2500	5	125
p.Kv7.2/Kv7.3	1,000k	7.5	125	1250:1250	7.5	125
p.N258K/Kv7.3	1,000k	7.5	125	1250:1250	7.5	125
p.G279D/Kv7.3	1,000k	7.5	125	1250:1250	7.5	125
Kv7.2/p.N258K/Kv7.3	1,000k	7.5	125	1250:625:625	7.5	125
Kv7.2/p.G279D/Kv7.3	1,000k	7.5	125	1250:625:625	7.5	125

b Immunofluorescence (12-well)

Condition	Cells	Working Lipofectamine 3000 Reagent			DNA Master mix	
		Lipofectamin3000 (uL)	Opti_MEM (uL)	Plasmids (ng)	P3000 (uL)	Opti_MEM (uL)
p.Kv7.2	300k	3	50	1000	2	50
p.Kv7.3	300k	3	50	1000	2	50
p.N258K	300k	3	50	1000	2	50
p.G279D	300k	3	50	1000	2	50
p.Kv7.2/Kv7.3	300k	3	50	500:500	3	50
p.N258K/Kv7.3	300k	3	50	500:500	3	50
p.G279D/Kv7.3	300k	3	50	500:500	3	50

c Western blotting (T75)

Condition	Cells	Working Lipofectamine 3000 Reagent			DNA Master mix	
		Lipofectamin3000 (uL)	Opti_MEM (uL)	Plasmids (mg)	P3000 (uL)	Opti_MEM (uL)
p.Kv7.2	5,000k	60	750	20	40	750
p.N258K	5,000k	60	750	20	40	750
p.G279D	5,000k	60	750	20	40	750
p.Kv7.2/Kv7.3	5,000k	60	750	10:10	40	750
p.N258K/Kv7.3	5,000k	60	750	10:10	40	750
p.G279D/Kv7.3	5,000k	60	750	10:10	40	750

Immunofluorescence

Protein localization studies, HEK293 cells growing on Poly-D-Lysin-coated (2mg/mL) coverslips were transiently transfected for 72 hours. After that, cells were fixed with 4% paraformaldehyde for 15 minutes. For homomeric condition; Kv7.2(WT) and mutants, tagged with GFP were mounted with ProLong Gold Antifade Mountant (Invitrogen# P36934). On the

other hand, heteromeric channels; Kv7.2/Kv7.3 (WT) and mutants, cells were permeabilized using 0.2% Triton X-100 in PBS for 20 minutes and blocked with 1% BSA for 1 hour at RT. Next, cells were incubated overnight at 4 °C, out of light with KCNQ3 polyclonal antibody (1:800) (Invitrogen# PA1-930) in 0.1% BSA, followed by 2 h at RT incubation with a Donkey Anti-Rabbit IgG H&L (Alexa Fluor 647, abcam) (1:500) in 0.1% BSA. Lastly, cells several were washed steps and mounted onto microscope slides. Confocal microscopic observations were performed with a Zeiss axio observer z1 microscope equipped with a 63x oil immersion lens. For images acquisition and analysis used The Zen 3.4 (blue edition) software.

Western blotting

In the study, proteins expression were divided into three parts: total protein lysates (TL), membrane-associated proteins (MP) and cytosol proteins (CP). First of all, 72 hours post-transfection, HEK293 cells (5×10^6 cells) in the growth medium were scraped by cell scraper on ice and centrifuge harvested at 300 g for 5 minutes. Then, cell pellets were washed by (1X) phosphate-buffered saline (PBS) and centrifuged at 300 g for 5 minutes. For total lysate proteins, cells were lysed in 500ul of RIPA buffer (Thermo Fisher, Waltham, MA, USA) containing 1X protease inhibitor cocktail (Thermo Scientific). Conversely, fractional proteins were extracted by Mem-PER Plus Membrane Protein Extraction Kit (Thermo Scientific). Briefly, 1.5mL of Cell Wash Solution washed cells and centrifuged at 300 g for 5 minutes. Next, cell pellets were incubated with 0.75mL of Permeabilization Buffer for 10 minutes at 4°C. After that, permeabilized cells were centrifuged at 16,000 g for 15 minutes keeping supernatant containing cytosolic proteins (CP). Meanwhile, the pellets were incubated by Solubilization Buffer for 30 minutes at 4°C that are membrane-associated proteins (MP). Secondly, western blot analysis, proteins (20 μ g/lane) from the total lysate and fractional proteins were resolved by SDS-Laemmli buffer (BIO-RAD) with 3% β -mercaptoethanol. After that, heating of proteins at 95 °C for 1 min, the samples was separated on 8% sodium dodecyl sulfate–polyacrylamide gel electrophoresis (SDS-PAGE) running at 80 V for 40 min and then at 90 V for 2.30 h. The proteins were transferred onto polyvinylidene difluoride PFDV membranes (Invitrogen). GAPDH was used as a loading control. The membranes were blocked in blocking agent (5% nonfat dry milk) for 1 h at RT and washed with washing buffer (Tris-buffered saline (TBS) + Tween 0.05%) four

times, each time 10 minutes. Then, they were incubated overnight at 4 °C with anti-Kv7.2 Rabbit mAb (1:500) (Cell Signaling Danvers, Massachusetts, USA) in 5% BSA and GAPDH Rabbit mAb (1:500) (Cell Signaling) in 5% BSA followed by Anti-rabbit IgG, HRP-linked Antibody (1:1000) (Cell Signaling) in 5% BSA for 1 h at RT. Finally, the blots were rinsed, and treated with SuperSignal West Pico PLUS Chemiluminescent Substrate (The Thermo Scientific). Protein bands visualized by chemiluminescence signals using Imaging Quant LAS4000.

Fluorescence activated cell sorting (FACS)

For electrophysiological analysis, 24 hours post-transfection, transfected cells were successfully identified by fluorescence activated cell sorting (FACS) (BD FACSAria II). Channel voltages were set as follows: Alexa Fluor 430 and 647. To detect KCNQ2-GFP expression and KCNQ3-DYKDDDDK Tag, conjugated to Alexa Fluor 647 (Cell Signaling Technology). Expressed cells were collected by collecting buffer (100X Fetal bovine serum and 1X Antibiotic-Antimycotic (Gibco). After that, cells were plated on 35-mm dishes coating with Poly-D-lysine (2mg/mL) hydrobromide at 37°C overnight.

Whole cell patch-clamp analysis

Electrophysiological analysis of the p.N258K and p.G279D mutant channels were performed by standard whole-cell patch-clamp technique. There investigated potassium currents (M-currents). Wild-types (p.Kv7.2 and p.Kv7.2/Kv7.3) were positive control channels. Non-transfected HEK293 cells were negative control channels because it had multiple endogenous Kv genes. Whole-cell patch-clamp technique used an Axopatch 200-B amplifier (Axon Instruments, Inc), controlled by a Digidata 1440A digitizer. The pCLAMP software ((Version 10, Axon Instruments, Inc)) was used for data acquisition and analysis. Briefly, transient transfected HEK293 cells, 24 h after fluorescence activated cell sorting (FACS). Expressed cells were covered at 2-2.5 ml/min with extracellular solution contained (in mM): 145 NaCl, 5 KCl, 2 CaCl₂, 1 MgCl₂, 10 glucose, and 10 HEPES, pH 7.3-7.4 titrated with NaOH; osmolality 315–320 mOsm/Kg. The borosilicate glass microelectrodes (BF150-86-10, Sutter/USA) has resistance of 1-3 MΩ when pipette intracellular solution contained (in mM) the following: 140 K-gluconate, 2 MgCl₂, 1 CaCl₂, 10 EGTA, 10 HEPES, and 10 Mg-ATP, pH 7.3-7.4 titrated with KOH;

osmolality 285–290 mOsm/Kg. Currents were recorded in response 1.3 s, voltage steps of potentials 10 mV, potentials ranging from –110 mV to +50 mV from a holding potential of –80 mV. Tail currents (deactivating) were recorded at –40 mV (Fig. 8).

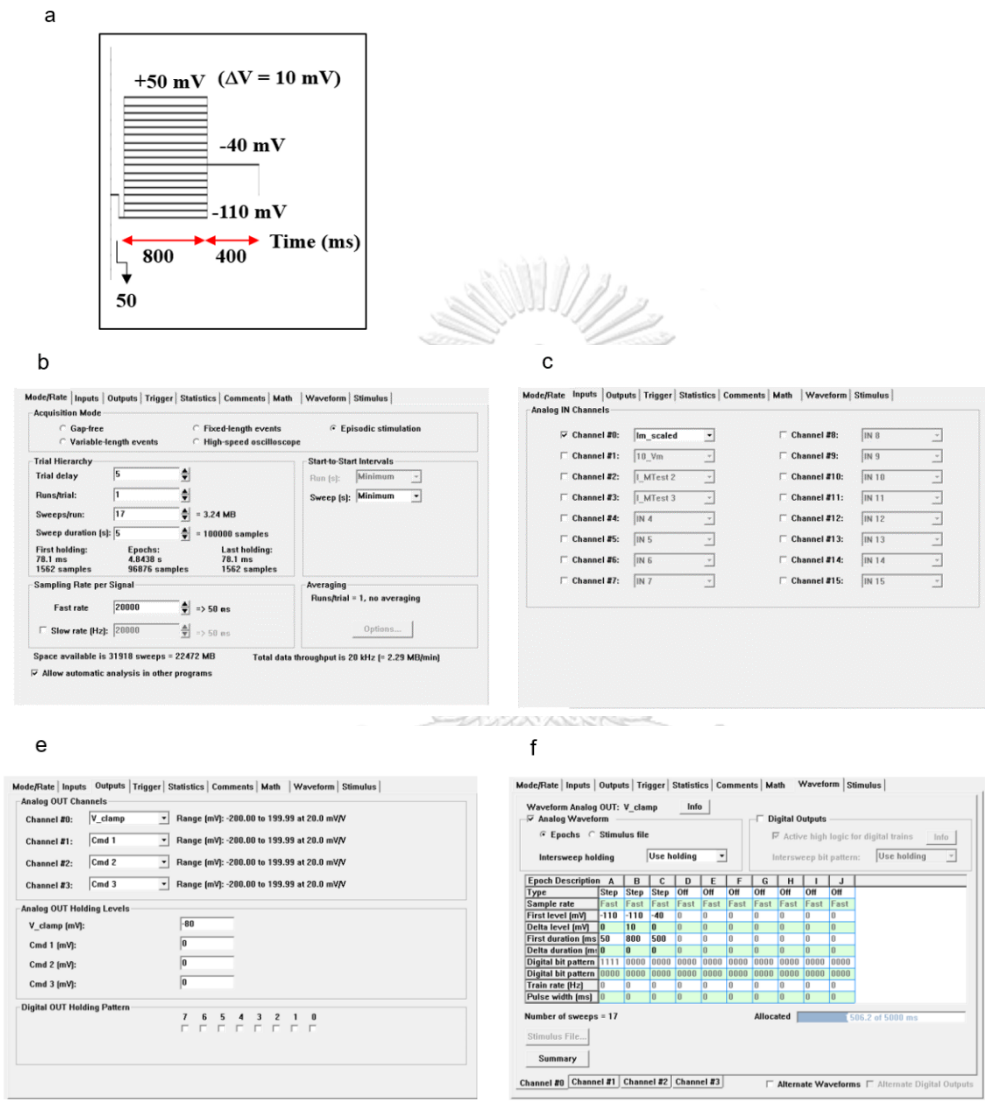


Figure 8 Setting protocol for whole-cell patch-clamp recording.

(a) Voltage steps of potentials for this study (b-f) Procedure for setting up protocols with Clampex software.

Data analysis

To examine the electrophysiological and potassium (K⁺) gating properties. Electrophysiological properties were demonstrated by representative raw M-current traces, the

current–voltage (I–V) curves used to estimate the conductance and reversal potential and M-current density used to estimate electrical capacitance (criteria of diagnosis for *KCNQ2*-epileptic disorders). It was calculated as peak current (pA) at +50 mV divided by the cell capacitance (pF). On the other hand, K⁺ gating properties were investigated by the half-activating voltage ($V_{1/2}$) detected depolarization of channels, the slope conductance (k) of channels. There were calculated by the Boltzmann function: $I = 1/[1+\exp(V_{1/2}-V)/k]$, $V_{1/2}$ = half-activating voltage, k = slope, at tail current amplitudes at – 40 mV. The membrane resistance (R_m) was calculated according to Ohm's law ($V= IR$), I is the current, V is the voltage and R is the resistance detected the resistance of the cell membrane when ions flow through it⁶⁵. The membrane time constant (τ) were calculated by $R_m \times C_m$, C_m is membrane capacitance detected time of change membrane potential⁶⁶.

Data are expressed as means \pm S.E.M. Statistical analyses were carried out using SPSS and GraphPad Prism 9.4.0. One-way ANOVA followed by Tukey's posttest. The number of samples (n) have been indicated in the figure legends. Statistical significance was defined by * $p < 0.05$, ** $p < 0.01$, *** $p < 0.001$.

Clinical features of the patients

One hundred and four unrelated families with infantile-onset drug-resistant epilepsy underwent exome and genome sequencing. 43% *De novo* pathogenic and likely pathogenic variants in the *KCNQ2* gene were identified in 9% (9/104) of the patients and account for 20% (9/44) of the neonatal-onset cases.

67% (6/9) of the patients with *KCNQ2*-related epilepsy were female. All of the patients were born at term. There was no family history of epilepsy or developmental delay. All of the patients had seizures onset during the neonatal period. Neuroimaging data were available in 7 out of 9 patients. 71% (5/7) patients showed unremarkable neuroimaging. The EEG data were available in eight patients (88%; 8/9). The findings included multifocal epileptiform discharges (63%; 5/8) and burst suppression pattern (37%; 3/8). The number of antiepileptic drugs used before genetic testing ranged from 2 to 6. The clinical characteristics of the patients are summarized in Supplementary Table S1.

Molecular characteristics

Seven *de novo* missense pathogenic and likely pathogenic variants were found in nine patients (Supplementary Table S1). The p.N258K and p.G279D variants have never been previously reported. Both variants occurred *de novo* (Fig 9a-b) and were not found in healthy population. In silico analysis using SIFT (<http://sift.jcvi.org/>); Polyphen-2, (<http://genetics.bwh.harvard.edu/pph2/>); M-CAP (<http://bejerano.stanford.edu/mcap/>); CADD (<https://cadd.gs.washington.edu/>; recommended pathogenicity threshold >20) predict the variants to be disease-causing (Supplementary Table S2). The Asparagine and glycine residue are located in the pore-loop domain of the Kv7.2 and are highly conserved across members of the Kv7 family (Fig 10a-b). We performed functional studies to confirm the pathogenicity of both variants.

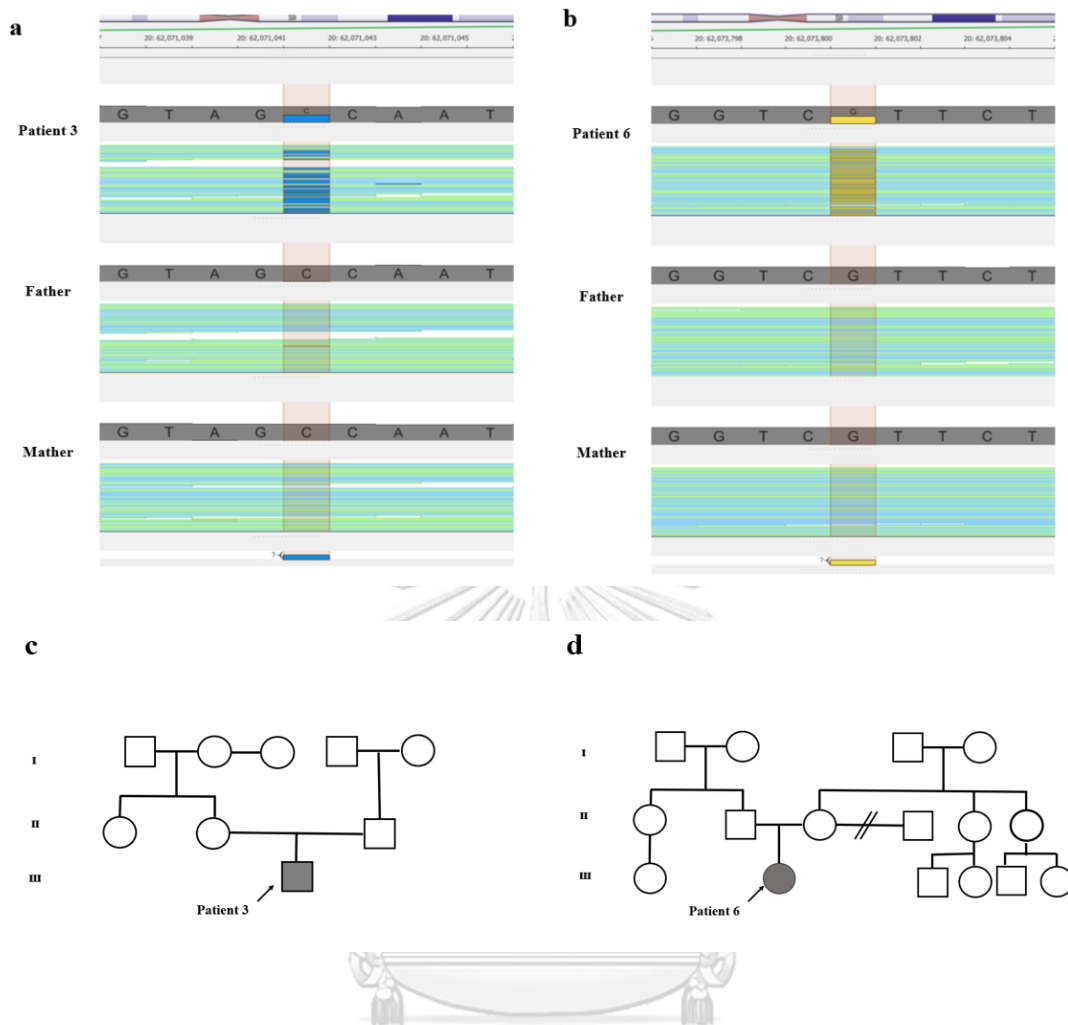


Figure 9 Sequence alignment of the patient's BAM file on Golden Helix Genome Browse 3.0.0 and pedigree of families

(a,b) The total yield of read depth was 104/85 (Reference/Alternate) for the p.N258K variant and 72/33 (Reference/Alternate) for the p.G279D variant. (b,d) **pedigree of families**, the solid black symbol is a family member with different KCNQ2-DEE. The open symbol represents a healthy family.

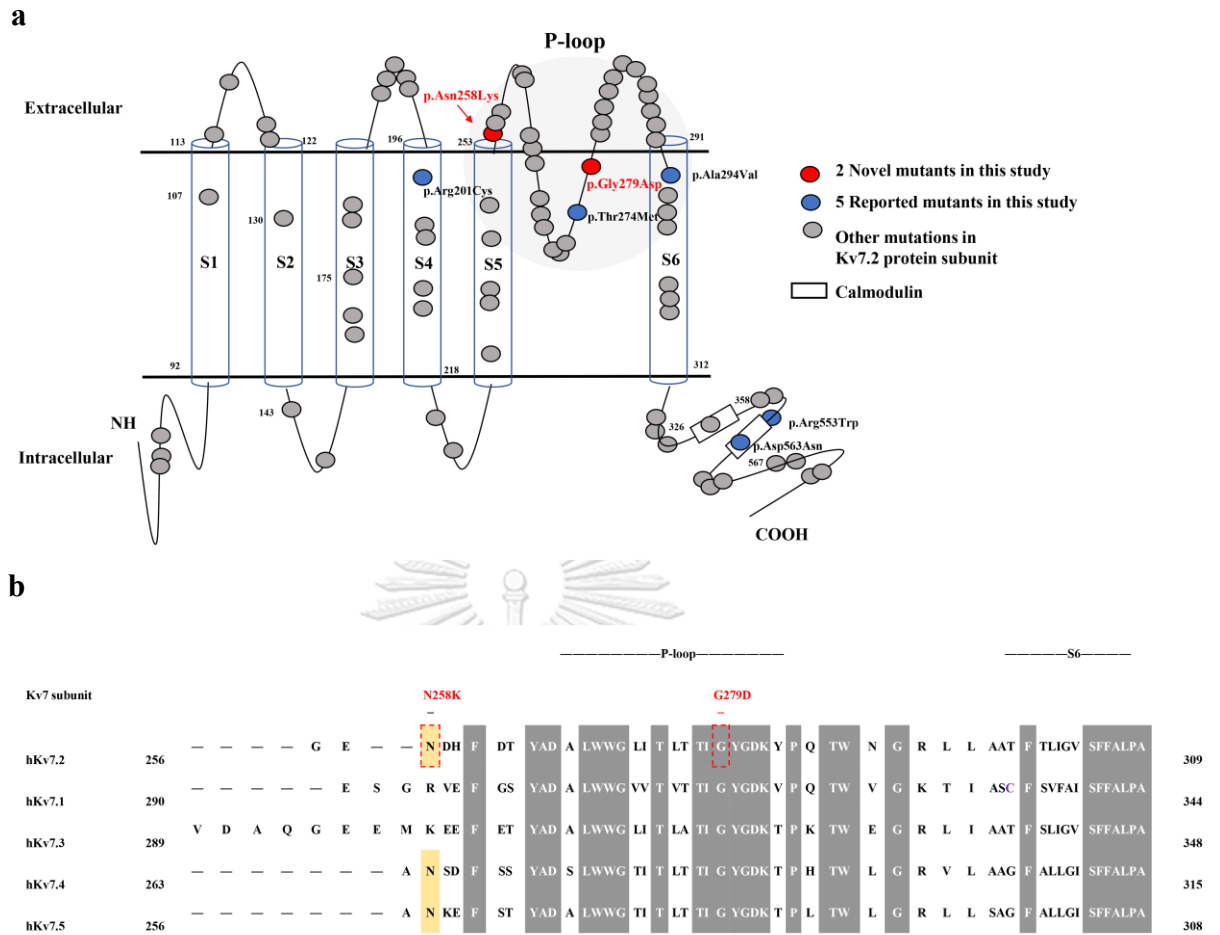


Figure 10 Schemes representation of Kv7 subunits with different mutation locations in Kv7.2 subunits. (a) Predicted positions of missense mutations in pore loop domain (p.N258K, p.G279D). (b) Alignment of human Kv7 subunits and location of amino acids mutated in the pore loop domain to the beginning of S6 among Kv7.2 subunits. Grey boxes are highly conserved sequence of Kv7 subunits. Yellow boxes are highly conserved in the voltage-gated K⁺ channel subunits.

Generated plasmid

1. Generated plasmid constructions; Kv7.2-GFP WT

The cloning of expressed genes and the polymerase chain reaction (PCR), two genetic engineering were used generating of Kv7.2-GFP WT plasmids which expressed *KCNQ2*-GFP fusion proteins. We amplified in-frame *KCNQ2* gene (Fig. 11a-b) and subcloned into the GFP-expression vector in Fig. 12.

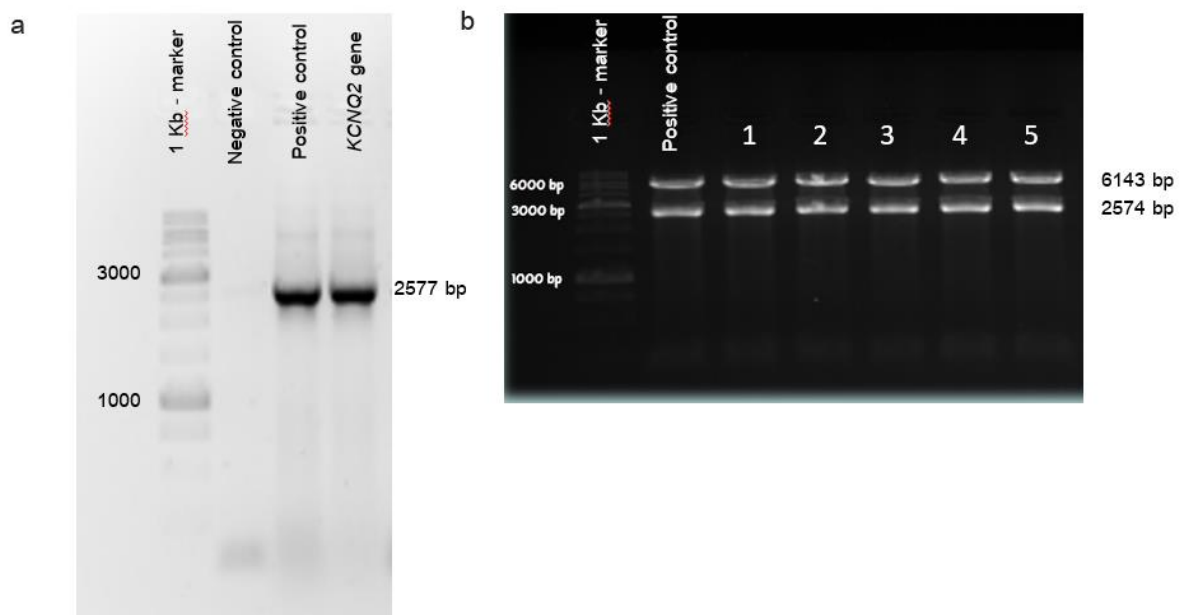


Figure 11 Polymerase chain reaction (PCR) of the KCNQ2 gene.

(a) The KCNQ2 gene product size (b) Restriction fragments length were digested by HindIII and EcoRV of verify the orientation of insert.

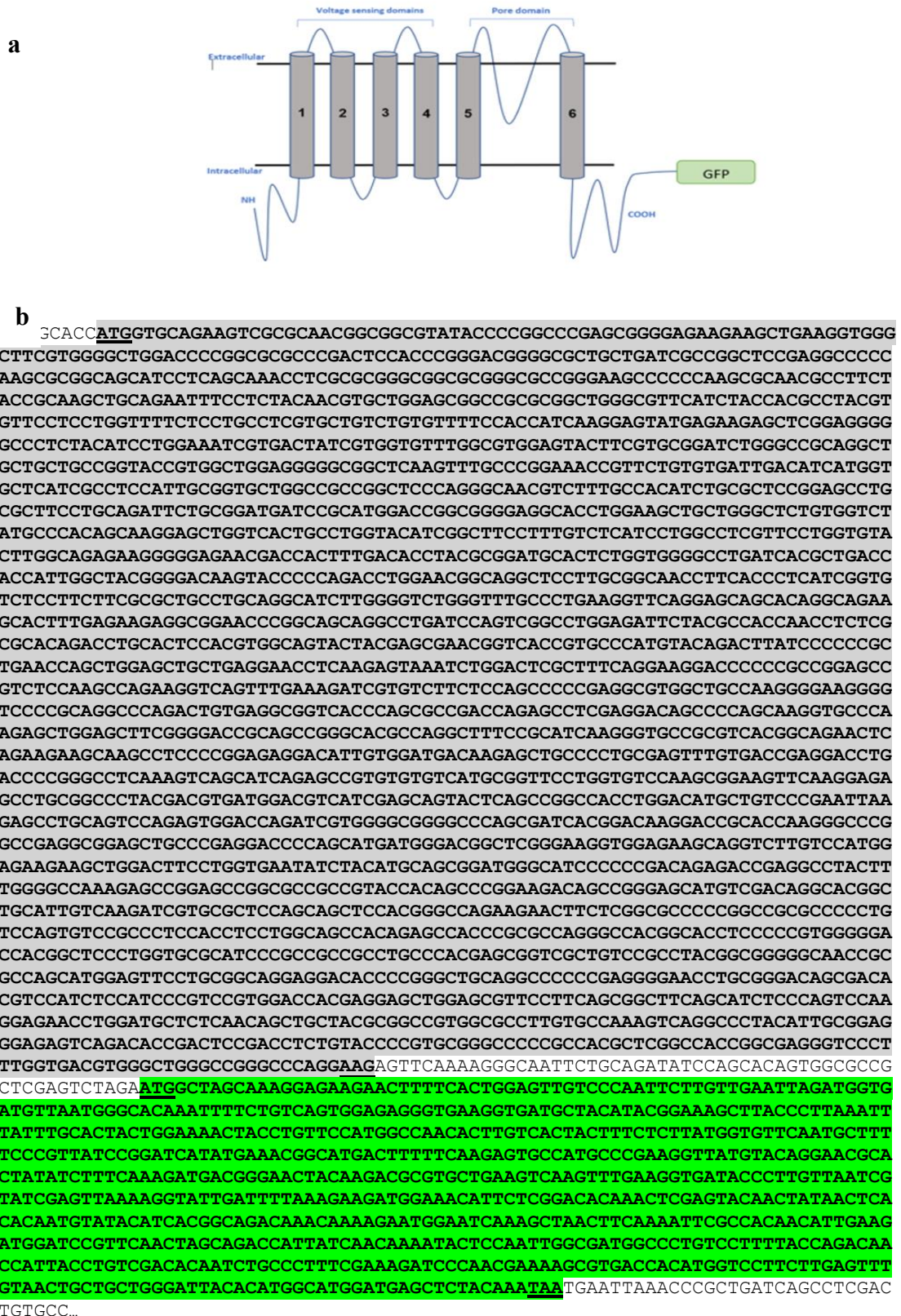


Figure 12 Plasmid constructions; Kv7.2-GFP WT.

(a) Schematic presentation of the Kv7.2-GFP subunit. (b) Sequence of the KCNQ2 gene deleted stop codon (dark box) and sequence of GFP- fusion (green box).

2. Generated plasmid constructions; mutants

The variants of interest were engineered in Kv7.2-GFP WT plasmids (variant 1; c.774C>G, p.N258K) and variant 2; c.836G>A, p.G279D) by QuikChange site-directed mutagenesis. Sanger sequencing was identified variant of mutant plasmids in Fig. 13.

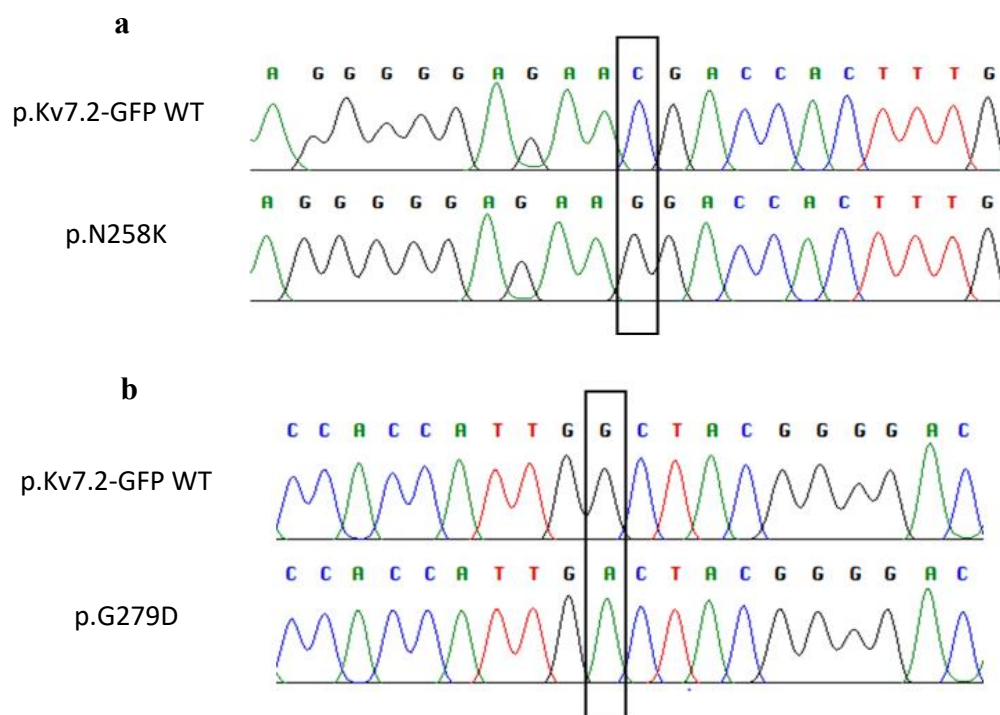


Figure 13 Chromatograms of sanger sequencing verified quality of the mutations

(a) p.N258K (b) p.G279D.

Fluorescent p.N258K and p.G279D reduces Kv7.2 plasma membrane expression

In comparisons to WT channels, plasma membrane expressions levels of p.N258K and p.G279D Kv7.2 were reduced (Fig. 14a). The co-assembly of Kv7.2 and Kv7.3 is crucial to their efficient trafficking and function, we thus determined the impact of p.N258K and p.G279D Kv7.2 in cells co-expressing WT Kv7.3 at a 1:1 ratio. In comparison to WT Kv7.2 and Kv7.3, Kv7.2 plasma membrane expression in cells expressing p.N258K and p.G279D Kv7.2 were reduced (Fig. 14b). This was also apparent in the Western blot analysis in which the membrane abundance of Kv7.2 in both p.N258K and p.G279D Kv7.2 were lower than WT Kv7.2 and when co-expressed with Kv7.3 (Fig. 15). This consistent with reduced plasma membrane expressions.

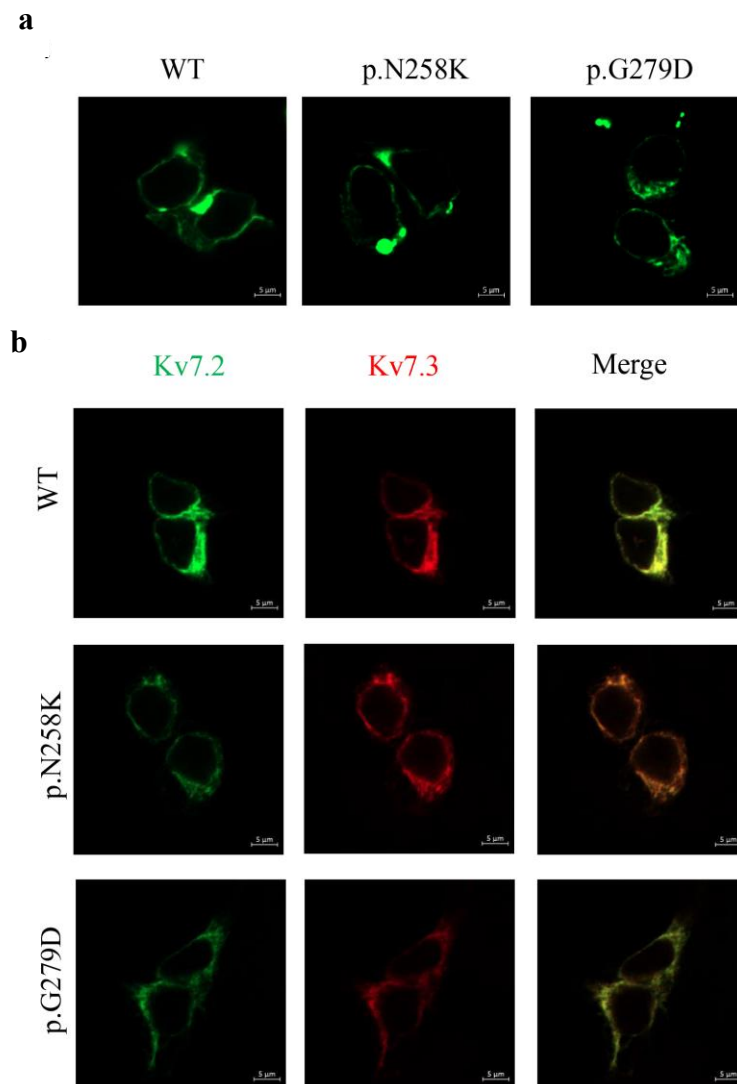


Figure 14 Immunofluorescence confocal microscopy showed localization on cell membranes.

(a) Non-permeabilized HEK293 cells expressing Kv7.2WT and mutant channels containing a GFP-tag in C-terminal; Kv7.2WT (left panel), p.N258K (middle panel) and p.G279D (right panel). Proteins are expressed in the same way on cell surfaces labeled by green signal. (b) Confocal images of GFP-tagged Kv7.2WT, p.N258K and p.G279D proteins (green signal). Cell surface was permeabilized and labeled by C-KCNQ3 antibodies (red signal). Kv7.2/Kv7.3WT and mutants were expressed at the cell surface of transfected HEK293 cells as shown by the merge (yellow signal). Scale bars 5 μ m.

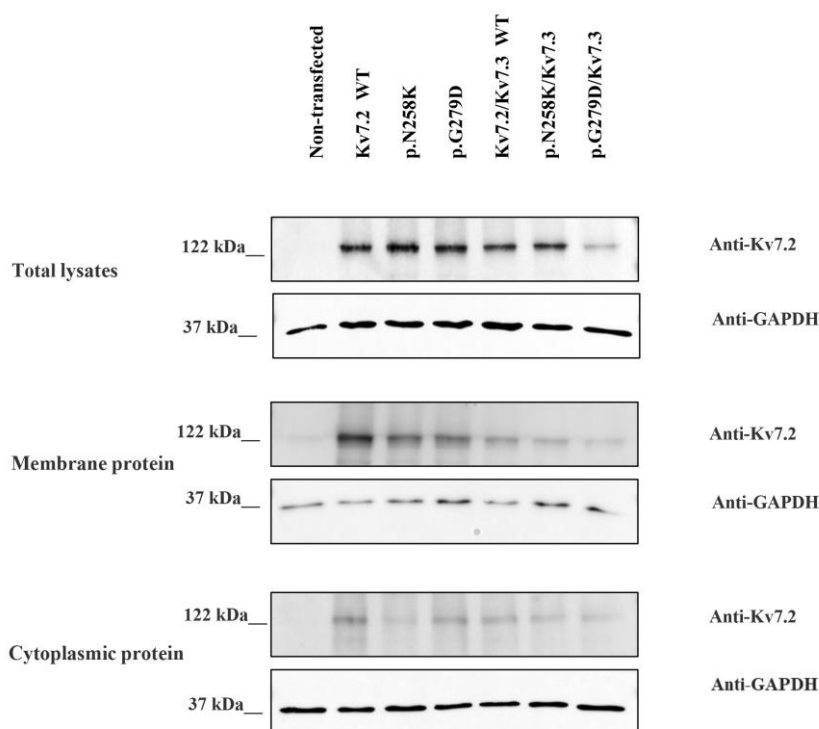


Figure 15 Western blots of Kv7.2 protein expressions in membrane, cytoplasmic and total cell lysate of cells expressing Kv7.2WT, p.N258K and p.G279D, Kv7.2/Kv7.3WT, or p.N258K or p.G279D co-expressed with Kv7.3. Non- transfected HEK293 cells was used as a negative control and GAPDH as a loading control.

Fluorescence activated cell sorting (FACS)

For electrophysiological analysis 48 h post-transfection. Cell expressions were successfully identified by fluorescence-activated cell sorting (FACS) (BD FACSAria II). To detect Kv7.2-tagged GFP expressions and Kv7.3-tagged DYKDDDDK, conjugated Alexa Fluor 647. Images presented plot of positive cells of GFP expressed on Q1 gate which were homotetrameric channels. Q2 gate were showed plot of heterotetrameric channels, presenting of positive cell of GFP and DYKDDDDK tags expression (Fig. 16).

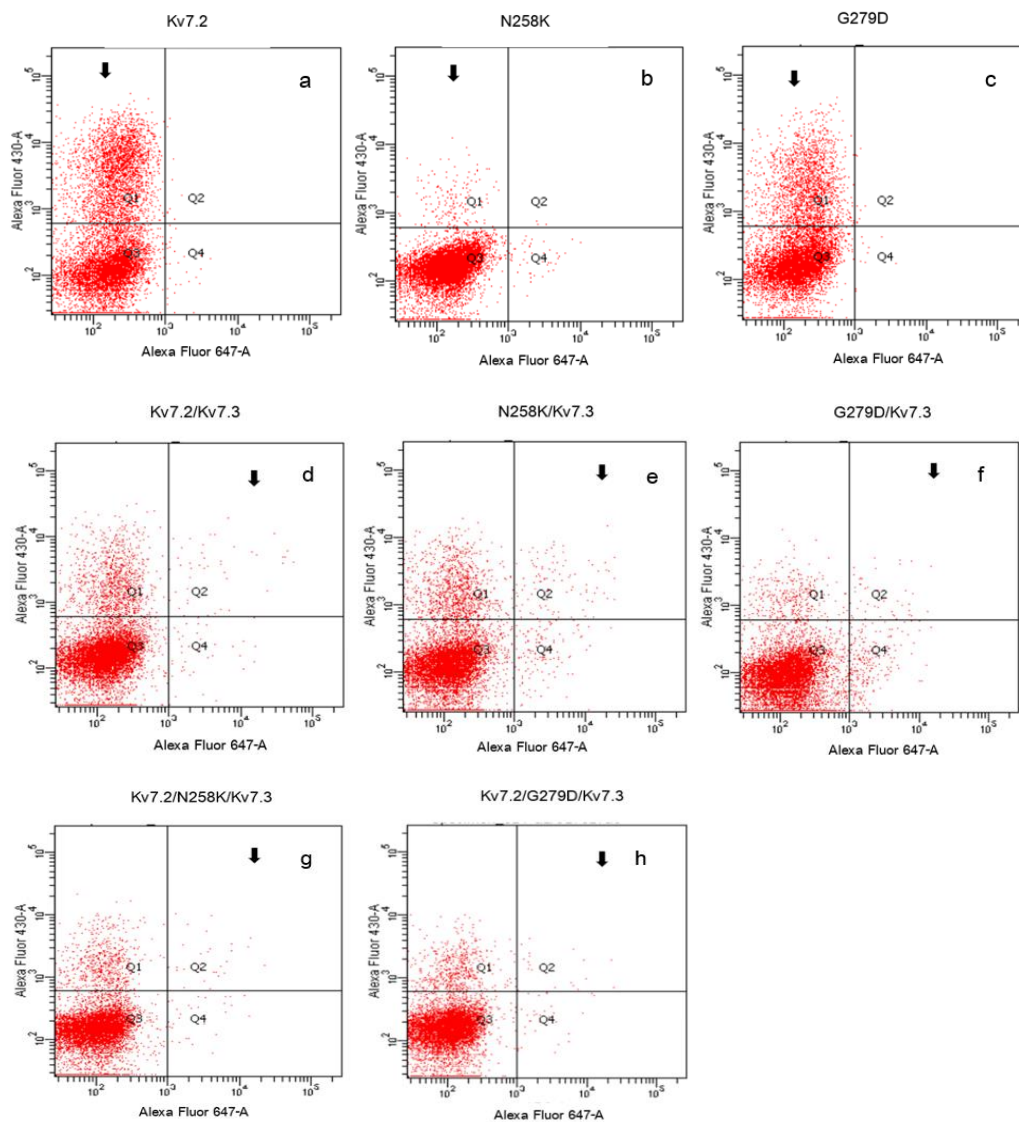


Figure 16 Histogram profiles of sorting gates used for FACS based on Alexa Fluor 430 and 647 channels. **(Panels a-c)** were used to define KCNQ2-GFP sorting gates, **(panels d-h)** were used to define Kv7.2-tagged GFP expressions and Kv7.3-tagged DYKDDDDK, conjugated to Alexa Fluor 647 sorting gates. These gates were positioned such that Q1: cells expressed GFP, Q2: cells expressed GFP& DYKDDDDK tag, Q3: non-transfected cell, Q4: cells expressed DYKDDDDK tag.

Electrophysiological properties of p.N258K and p.G279D mutations in Kv7.2.

We analyzed electrophysiological function of pathogenic Kv7.2 variants p.N258K and p.G279D that was performed by whole-cell patch clamp recording in expression transfected HEK293 cells. Expression cells were identified by fluorescence-activated cell sorting (FACS). To determine affected function of mutant channels after transfection of homotetrameric variants. Moreover, most patients diagnosed with *KCNQ2*-associated epileptic disorders were autosomal dominant heterozygous epilepsy. Therefore, we performed patch clamp repeat recordings, in which co-expressing with Kv7.2WT, p.N258K, p.G279D and Kv7.3WT at homologous heterotetrameric channels; 1:1 ratio (1.25 μg : 1.25 μg) and heterozygous heterotetrameric channels 1:1:2 ratio (0.625 μg : 0.625 μg : 1.25 μg). These ratios mimic the expression of the physiological heterotetrameric channels and used to study a dominant negative effect on the M-channel activity⁶⁷. Non-transfected HEK293 cells were used negative control (n = 22 cells)⁶⁸.

To examine the electrophysiological parameters that consist of electrophysiological properties and potassium (K⁺) gating properties. Electrophysiological properties were demonstrated function of mutant channels by representative raw M-current traces, the current-voltage (I-V) curves used to estimate the conductance and reversal potential and M-current density used to estimate electrical capacitance. On the other hand, K⁺ gating properties were investigated by the half-activating voltage ($V_{1/2}$) detected depolarization of channels, the slope conductance (k) of channels. The membrane resistance (R_m) detected the resistance of the cell membrane when ions flow through it. The membrane time constant (*Tau*) detected time of change the membrane potential to return to the "resting state".

1. Electrophysiological function in the novel p.N258K mutate on of Kv7.2

To analyze the electrophysiological functions of p.N258K, whole-cell patch clamp was performed in homotetrameric channels (p.N258K Kv7.2; n=15 cells) and heterotetrameric channels (p.N258K/Kv7.3; n= 15 cells and Kv7.2/p.N258K/Kv7.3; n= 13 cells) channels versus WT (Kv7.2; n = 18 cells and Kv7.2/Kv7.3; n = 22 cells). Cells expressing p.N258K exhibited lower M-current amplitude almost ~40-50% (Fig 17 b-g) and current density (reduction of about ~51.97 % in p.N258K, ~54.09 % in p.N258K/Kv7.3 and ~51.11 % in Kv7.2/p.N258K/Kv7.3) when compared to Kv7.2WT and Kv7.2/Kv7.3WT (Fig 18). The conductance-voltage relationship was showed significantly reduce in conductance at conditional voltage -50 mV to +50 mV (Fig. 19a-b & Supplementary Fig. S2-3) and shifted significantly towards depolarized voltages for 0.87 mV in p.N258K, 2.24 mV in p.N258K/Kv7.3 and 1.18 mV in Kv7.2/p.N258K/Kv7.3 compared to WT, resulting in a more positive half-activating voltages ($V_{1/2}$) and lower slope conductance (K) (Fig. 20a-b, & Supplementary Table. S3). But there was no significant increase in reversal potential when compared with WT which was equilibrium gradient of K⁺ ions (Fig. 19c & Supplementary Table. S3). Input resistance and time constant (*Tau*) in cells expressing p.N258K were significantly higher than in WT cells (Fig. 21a-b & Supplementary Table. S3).

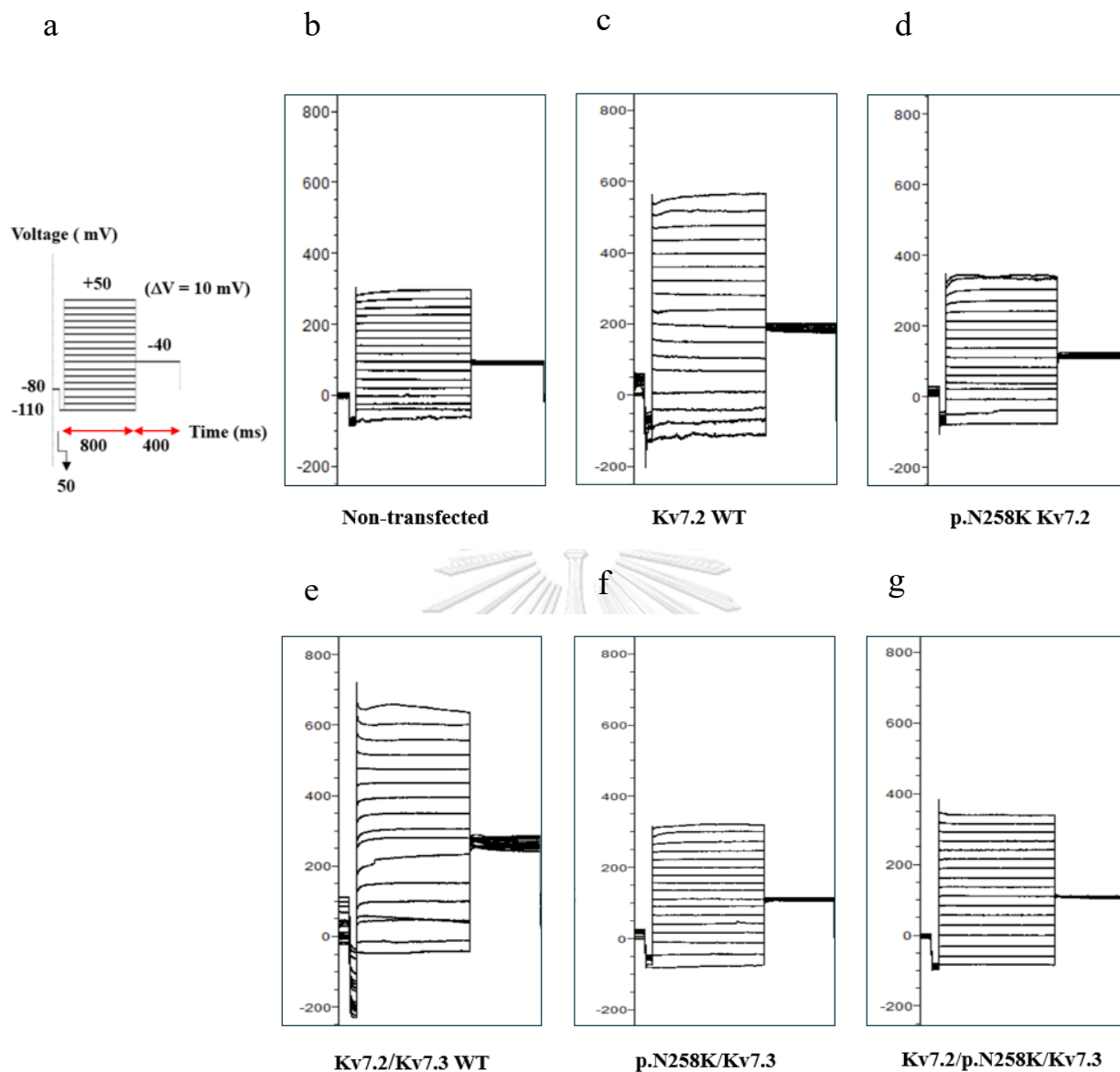


Figure 17 Representative raw current traces for homotetrameric and heterotetrameric in p.N258K channels.

(a) Voltage step protocol (b-g) Representative current traces of non-transfected (n = 22), Kv7.2WT (n = 18), p.N258K Kv7.2 (n = 15), Kv7.2/Kv7.3WT (n = 22), p.N258K /Kv7.3 (n = 14), Kv7.2/p.N258K/Kv7.3 (n = 13) in response to the assigned voltage protocols.

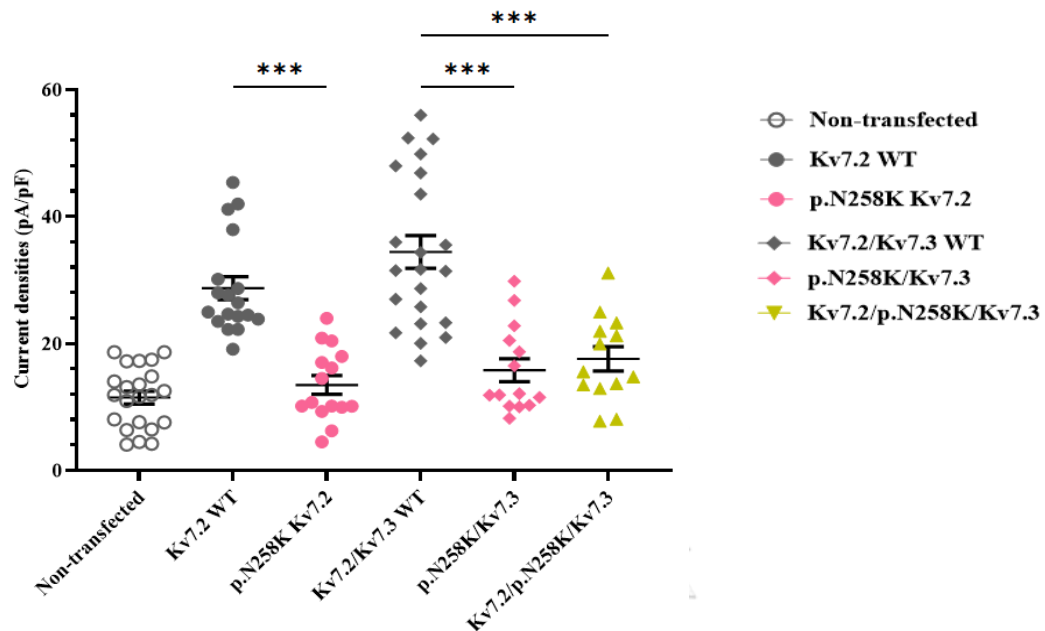


Figure 18 Comparison of average peak M-current densities (pA/pF) at +50 mV in homotetrameric and heterotetrameric of p.N258K channels.

The mean scores were 13.46 ± 1.48 pA/pF in p.N258K Kv7.2 and 28.02 ± 1.81 pA/pF in Kv7.2WT, with a significant difference between the groups ($p < 0.001$). Post hoc analysis showed that the mean scores of p.N258K Kv7.2 channels was significantly lower than in Kv7.2WT ($p < 0.001$). On the other hand, the mean scores were 15.79 ± 1.83 pA/pF in p.N258K/Kv7.3, 17.58 ± 1.89 pA/pF in Kv7.2/p.N258K/Kv7.3 and 34.40 ± 4.23 pA/pF in Kv7.2Kv7.3WT, with a significant difference between the groups ($p < 0.001$). Post hoc analysis revealed that the mean scores of p.N258K/KV7.3 and Kv7.2/p.N258K/Kv7.3 channels were dramatically two-fold lower than in Kv7.2/Kv7.3WT ($p < 0.001$ and $p < 0.001$, respectively). Statistically significant differences are indicated by * $p < 0.05$, ** $p < 0.01$, *** $p < 0.001$ based on one-way ANOVA Tukey test.

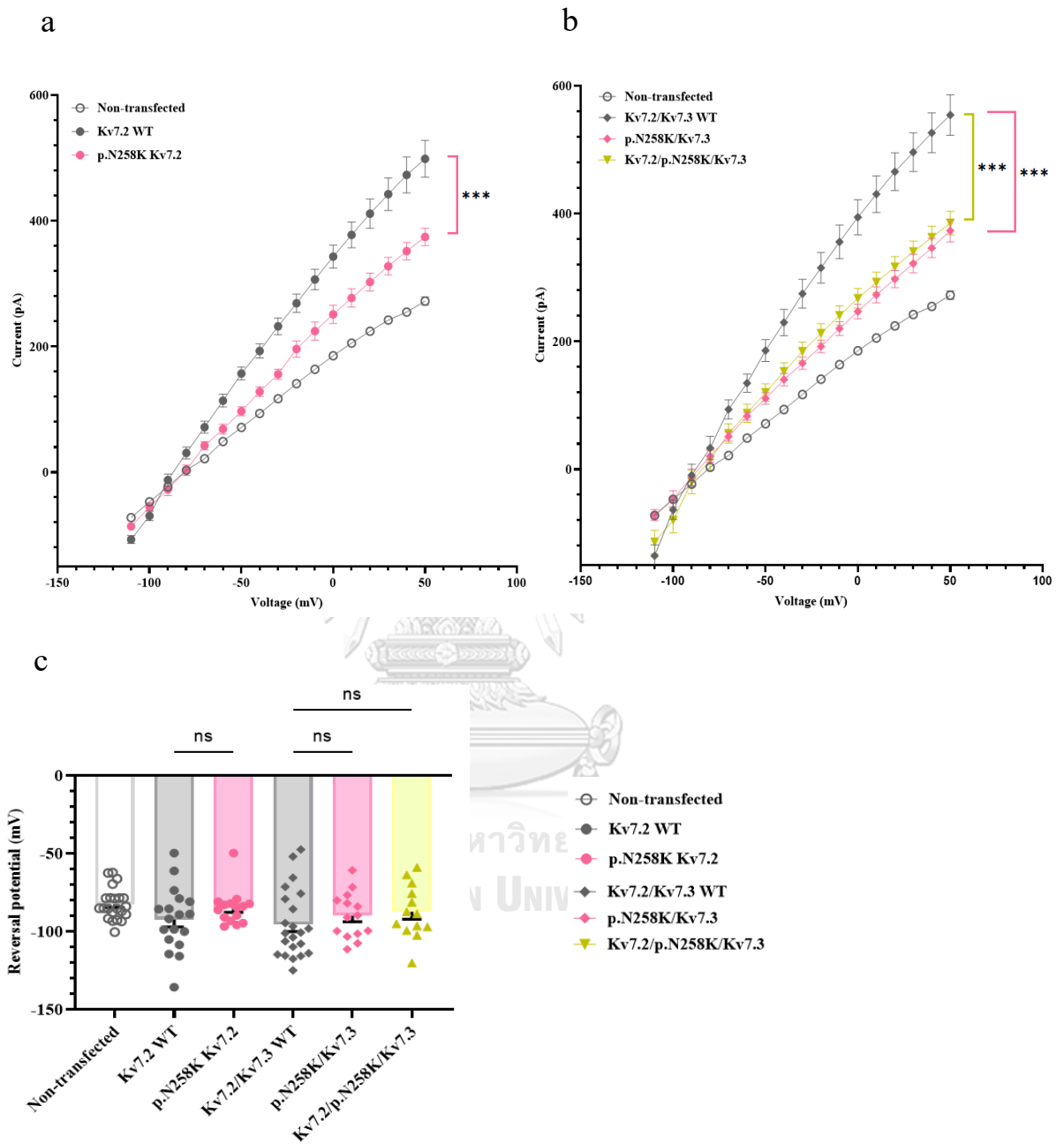


Figure 19 Analysis of the current–voltage (I–V) relationships (from -110 to $+50$ mV) and comparison of reversal potential in homotetrameric and heterotetrameric of p.N258K channels.

(a) The current–voltage (I–V) curves of p.N258K at conditional voltage -50 mV to $+50$ mV differed significantly between groups ($p < 0.001$). Post hoc analysis showed that the mean scores of p.N258K Kv7.2 channels was significantly lower than in Kv7.2.WT ($p < 0.001$) (b) The current–voltage (I–V) curves of p.N258K/Kv7.3 and Kv7.2/p.N258K/Kv7.3 at

conditional voltage -50 mV to +50 mV differed significantly between groups ($p < 0.001$). Post hoc analysis showed that the mean scores of p.N258K/Kv7.3 and Kv7.2/p.N258K/Kv7.3 channels were significantly lower than in Kv7.2/Kv7.3WT ($p < 0.001$ and $p < 0.001$, respectively). (c) Reversal potential were -84.78 ± 2.92 mV in p.N258K Kv7.2 and -92.30 ± 4.79 mV in Kv7.2WT, with a no significant difference between the groups ($p = 0.307$) and were -89.83 ± 3.94 mV in p.N258K/Kv7.3, -86.57 ± 4.71 mV in Kv7.2/p.N258K/Kv7.3 and -95.31 ± 4.63 mV in Kv7.2/Kv7.3WT, with a no significant difference between the groups ($p = 0.602$). Statistically significant differences are indicated by * $p < 0.05$, ** $p < 0.01$, *** $p < 0.001$, ns = no significant based on one-way ANOVA Tukey test.

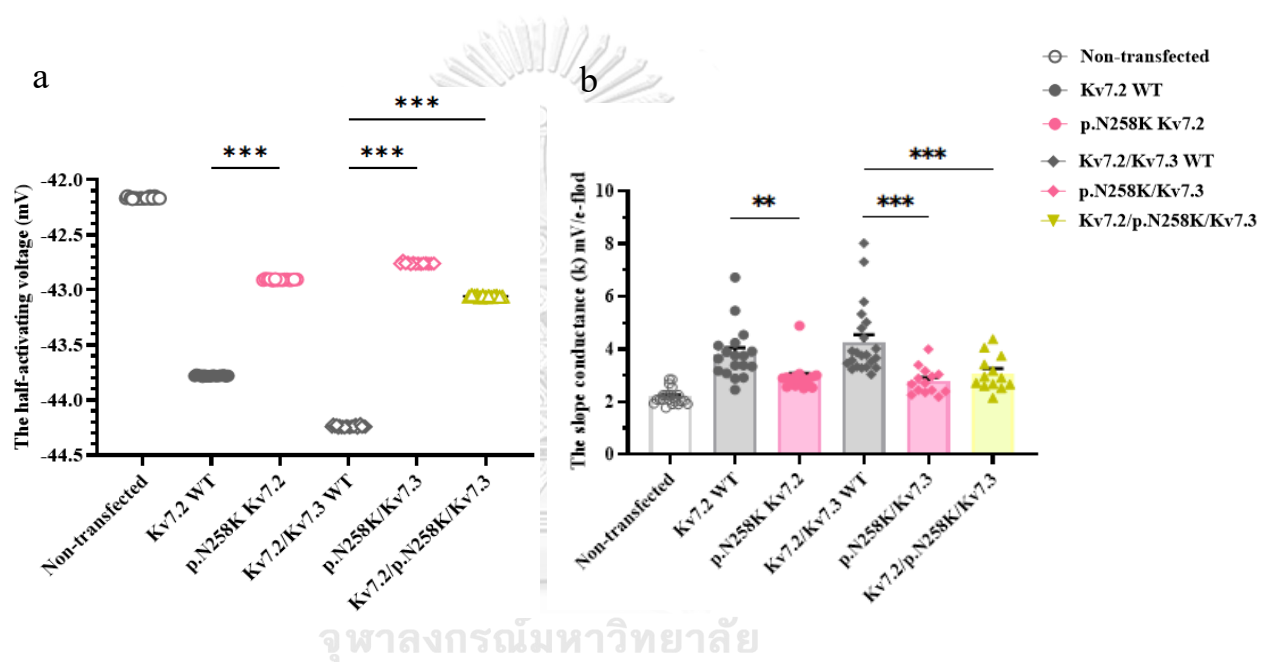


Figure 20 Comparison of K⁺ gating properties in homotetrameric and heterotetrameric p.N258K channels.

(a) The mean scores of the half-activating voltage ($V_{1/2}$) of homotetrameric channels were -42.91 ± 0.0013 mV in p.N258K Kv7.2 and -43.78 ± 0.0011 mV in Kv7.2WT, with a significant difference between the groups ($p < 0.001$). Post hoc analysis showed that the mean scores of p.N258K Kv7.2 channels was significantly increase when compared with Kv7.2WT ($p < 0.001$) while heterotetrameric channels were -42.76 ± 0.0021 mV in p.N258K/Kv7.3, -43.06 ± 0.0017 mV in Kv7.2/p.N258K/Kv7.3 and -44.24 ± 0.0019 mV in Kv7.2/Kv7.3WT, with a significant difference between the groups ($p < 0.001$). Post hoc analysis revealed significant increase when compared with Kv7.2/Kv7.3WT ($p < 0.001$ and $p < 0.001$, respectively) (b) The mean scores of the slope conductance (k) of homotetrameric channels were 2.93 ± 0.15 mV/e-fold in p.N258K Kv7.2 and 3.82 ± 0.24 mV/e-fold in Kv7.2WT, with a significant difference between the groups ($p < 0.001$). Post hoc analysis showed that the mean scores of p.N258K Kv7.2 channels was significantly decrease when compared with Kv7.2WT (p

= 0.002) while heterotetrameric channels were 2.78 ± 0.14 mV/e-fold in p.N258K/Kv7.3, 3.08 ± 0.18 mV/e-fold in Kv7.2/p.N258K/Kv7.3 and 4.26 ± 0.28 mV/e-fold in Kv7.2/Kv7.3WT, with a significant difference between the groups ($p < 0.001$). Post hoc analysis revealed that the mean scores of p.N258K/Kv7.3 and Kv7.2/p.N258K/Kv7.3 channels were significantly decrease when compared with Kv7.2/Kv7.3WT ($p < 0.001$ and $p = 0.002$, respectively).

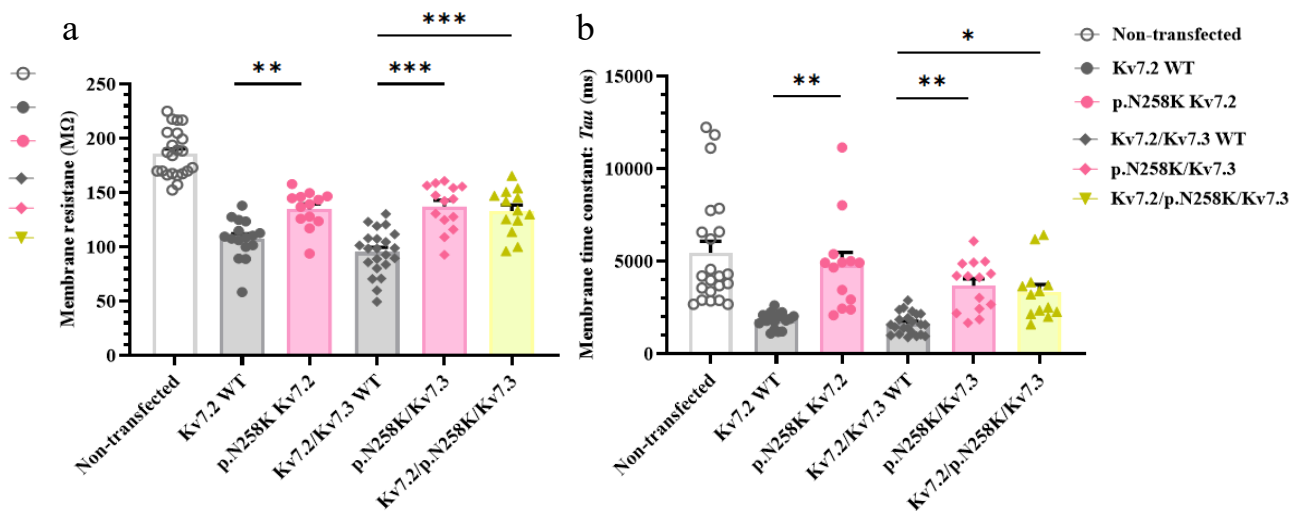


Figure 21 Comparison of the membrane resistance (Rm) and the membrane time constant (Tau) in homotetrameric and heterotetrameric of p.N258K channels.

(a) the mean scores of the membrane resistance (Rm) of homotetrameric channels were 135.65 ± 4.21 MΩ in p.N258K Kv7.2 and 105.41 ± 4.72 MΩ in Kv7.2WT, with a significant difference between the groups ($p < 0.001$). Post hoc analysis showed that the mean scores of p.N258K Kv7.2 expressed cells was significantly increase when compared with Kv7.2WT ($p = 0.003$) whereas heterotetrameric channels were 137.32 ± 5.59 MΩ in p.N258K/Kv7.3, 133.06 ± 5.78 MΩ in Kv7.2/p.N258K/Kv7.3 and 95.37 ± 4.41 MΩ in Kv7.2/Kv7.3WT, with a significant difference between the groups ($p < 0.001$). Post hoc analysis revealed that the mean scores of p.N258K/Kv7.3 and Kv7.2/p.N258K/Kv7.3 expressed cells were significantly increase when compared with Kv7.2/Kv7.3WT expressed cells ($p < 0.001$ and $p < 0.001$, respectively). (b) the mean scores of the membrane time constant (Tau) of homotetrameric channels were 4550.06 ± 621.66 ms in p.N258K Kv7.2 and 1889.149 ± 97.66 ms in Kv7.2WT, with a significant difference between the groups ($p < 0.001$). Post hoc analysis showed that the mean scores of p.N258K Kv7.2 expressed cells was significantly higher than in Kv7.2WT ($p = 0.005$) while, heterotetrameric channels were 3690 ± 364.38 ms in p.N258K/Kv7.3, 3337.08 ± 418.03 ms in Kv7.2/p.N258K/Kv7.3 and 1637.05 ± 122.93 ms in Kv7.2/Kv7.3WT, with a significant difference

between the groups ($p < 0.001$). Post hoc analysis revealed that the mean scores of p.N258K/Kv7.3 and Kv7.2/p.N258K/Kv7.3 expressed cells were significantly higher than in Kv7.2/Kv7.3WT ($p = 0.009$, $p = 0.05$, respectively). Statistically significant differences are indicated by * $p < 0.05$, ** $p < 0.01$, *** $p < 0.001$.

2. Electrophysiological function in the novel p.G279D mutate on of Kv7.2

The finding of patch-clamp showed defect in electrophysiological functions of p.G279D, whole-cell patch clamp was performed in homotetrameric (p.G279D Kv7.2; $n = 15$ cells) and heterotetrameric channels (p.G279D/Kv7.3; $n = 14$ cells and Kv7.2/p.G279D/Kv7.3; $n = 14$ cells) channels versus WT (Kv7.2WT; $n = 18$ cells and Kv7.2/Kv7.3WT; $n = 22$ cells). Cells expressing p.G279D exhibited lower M-current amplitude (almost ~ 20 -30%) (Fig.22b-g). and current density reduction of about $\sim 49.36\%$ in p.G279D Kv7.2, $\sim 51.49\%$ in p.G279D/Kv7.3 and $\sim 56.73\%$ in Kv7.2/p.N258K/Kv7.3 when compared to Kv7.2WT and Kv7.2/Kv7.3WT (Fig 23). The conductance-voltage relationship was showed significantly reduce in conductance at conditional voltage -50 mV to +50 mV (Fig. 24a-b & Supplementary Fig. S2-3) and shifted significantly towards depolarized voltages for 0.61 mV in p.G279D Kv7.2, 1.23 mV in p.G279D/Kv7.3 and 1 mV in Kv7.2/p.G279D/Kv7.3 compared to WT, resulting in a more positive half-activating voltages ($V_{1/2}$) and lower slope conductance (K) (Fig. 25a-b, & Supplementary Table. S3). But there was no significant increase in reversal potential when compared with WT which was equilibrium gradient of K⁺ ions (Fig. 24c & Supplementary Table. S3). Input resistance in cells expressing p.N258K were significantly higher than in WT cells while time constant (*Tau*) were increased in p.G279D Kv7.2 and p.G279D Kv7.2/Kv7.3 (Fig. 26a-b & Supplementary Table. S3).

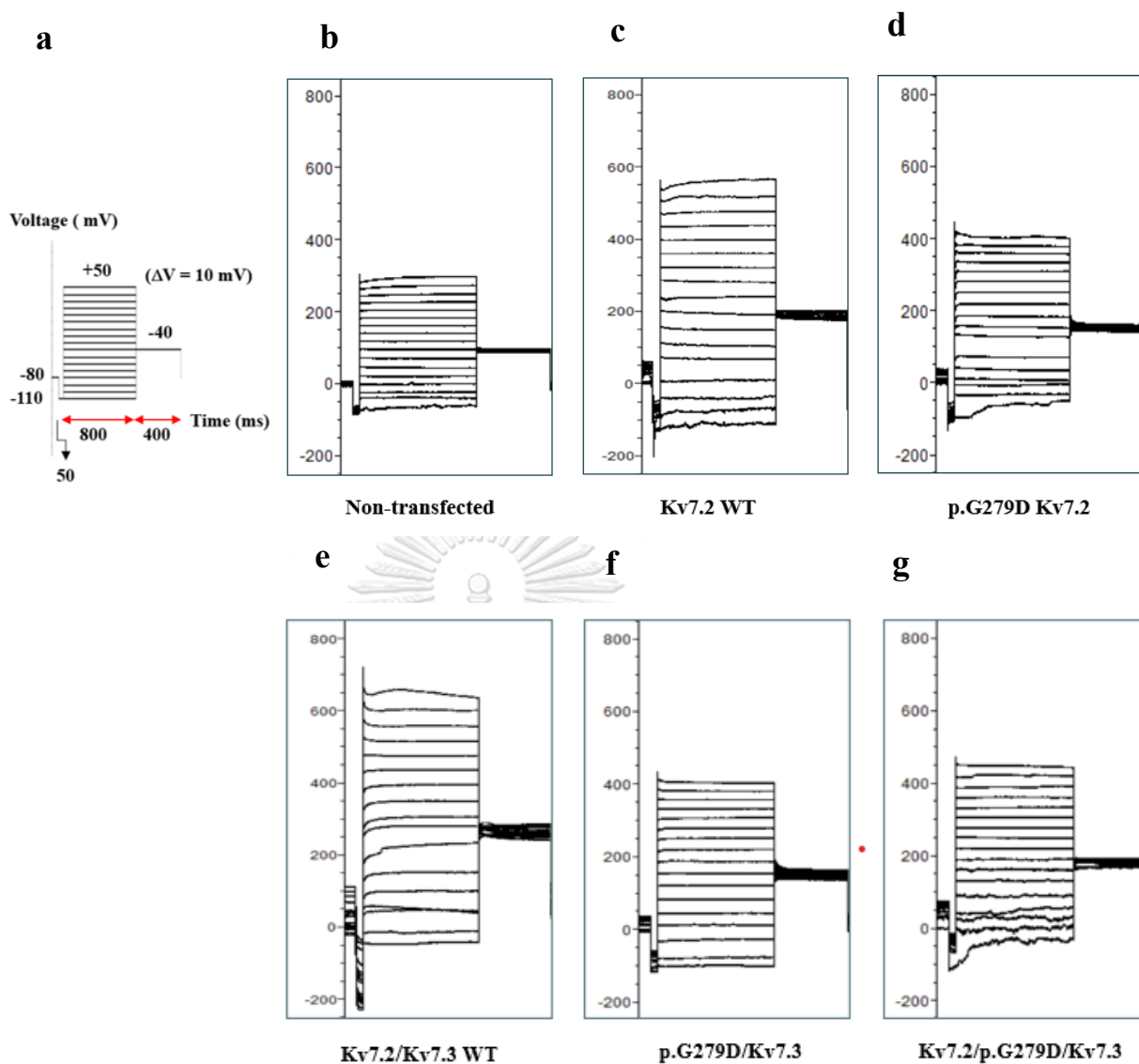


Figure 22 Representative raw current traces for homotetrameric and heterotetrameric in p.G279D channels.

(a) Voltage step protocol (b-g) Representative current traces of non-transfected (n = 22), Kv7.2WT (n = 18), p.G279D Kv7.2 (n = 15), Kv7.2/Kv7.3 WT (n = 22), p.G279D/Kv7.3 (n = 14), Kv7.2/p.G279D/Kv7.3 (n = 14) in response to the assigned voltage protocols.

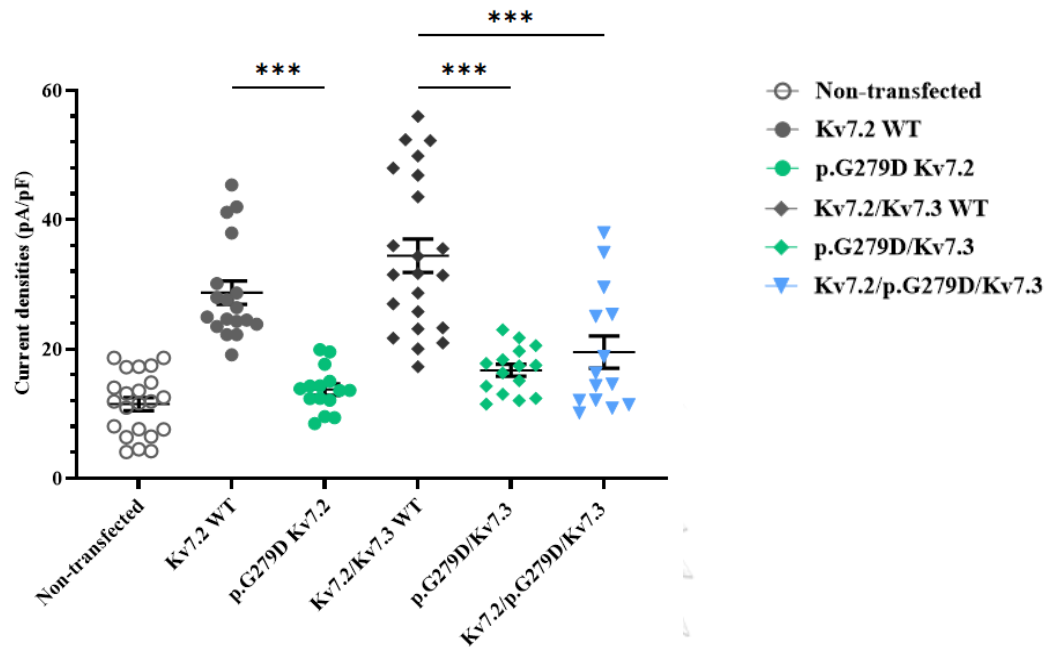


Figure 23 Comparison of average peak M-current densities (pA/pF) in homotetrameric and heterotetrameric of p.G279D channels.

The mean scores were 14.19 ± 1.03 pA/pF in p.G279D Kv7.2 and 28.02 ± 1.81 pA/pF in Kv7.2WT, with a significant difference between the groups ($p < 0.001$). Post hoc analysis showed that the mean scores of p.G279D Kv7.2 channels was significantly lower than in Kv7.2WT ($p < 0.001$). On the other hand, The mean scores were 16.69 ± 0.94 pA in p.G279D/Kv7.3, 19.52 ± 2.51 pA in Kv7.2/p.G279D/Kv7.3 and 34.40 ± 4.23 pA/pF in Kv7.2Kv7.3WT, with a significant difference between the groups ($p < 0.001$). Post hoc analysis revealed that the mean scores of p.G279D/Kv7.3 and Kv7.2/p.G279D/Kv7.3 channels were dramatically two-fold lower than in Kv7.2/Kv7.3WT ($p < 0.001$ and $p < 0.001$, respectively). Statistically significant differences are indicated by * $p < 0.05$, ** $p < 0.01$, *** $p < 0.001$ based on one-way ANOVA Tukey test.

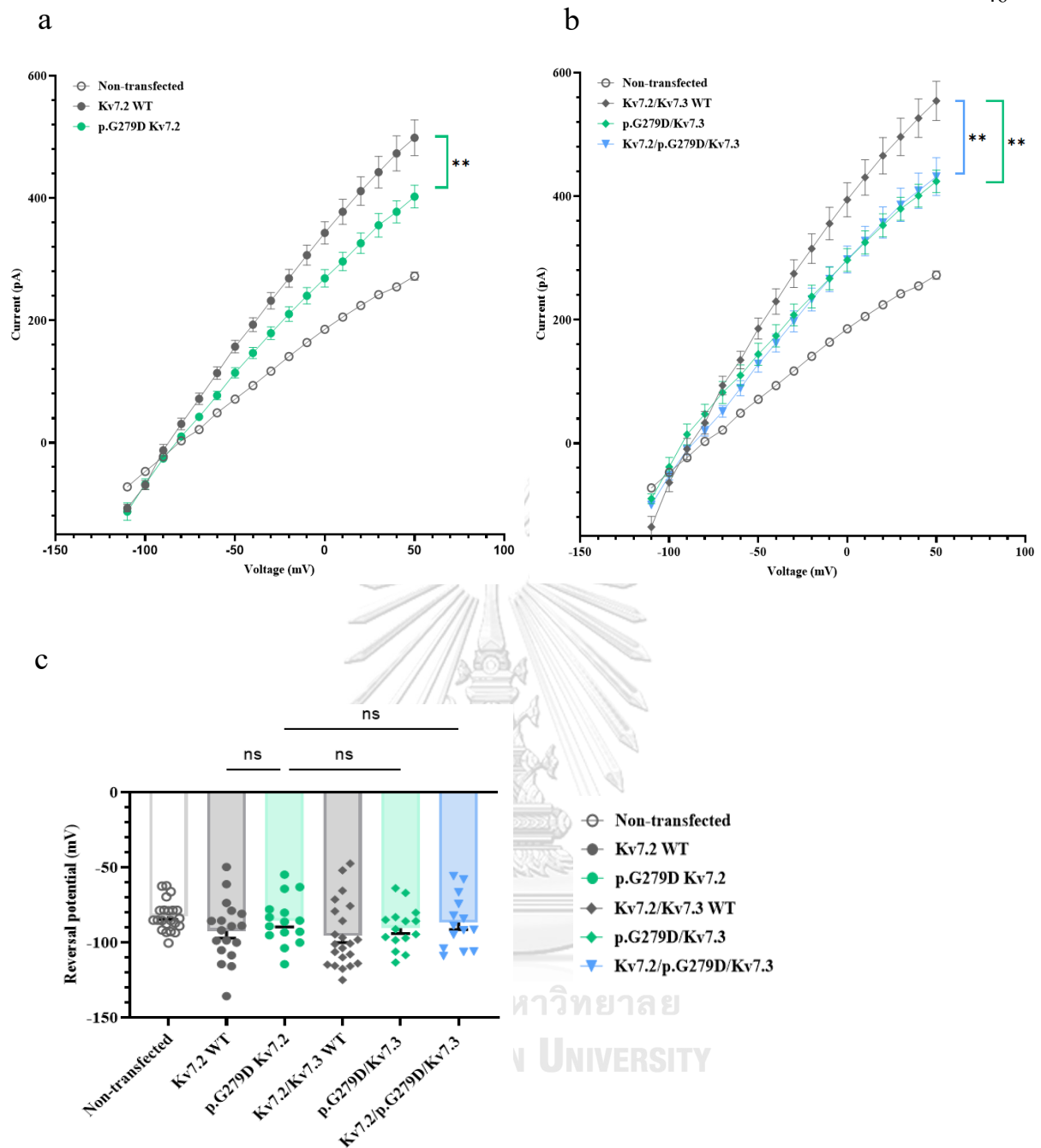


Figure 24 Analysis of the current–voltage (I–V) relationships (from -110 to $+50$ mV) and comparison of reversal potential in homotetrameric and heterotetrameric of p.G279D channels.

(a) The current–voltage (I–V) curves of p.G279D at conditional voltage -50 mV to $+50$ mV differed significantly between groups ($p < 0.001$). Post hoc analysis showed that the mean scores of p.G279D Kv7.2 channels was significantly lower than in Kv7.2WT ($p < 0.01$) (b) The current–voltage (I–V) curves of p.G279D/Kv7.3 and Kv7.2/p.G279D/Kv7.3 at conditional voltage -50 mV to $+50$ mV differed significantly between groups ($p < 0.001$). Post hoc analysis showed that the mean scores of p.G279D/Kv7.3 and Kv7.2/p.G279D/Kv7.3 channels were significantly lower than in Kv7.2/Kv7.3WT ($p < 0.01$ and $p < 0.01$,

respectively). (c) Reversal potential were -85.51 ± 4.13 mV in p.G279D Kv7.2 and -92.30 ± 4.79 mV in Kv7.2WT, with a no significant difference between the groups ($p = 0.307$) and were -90.33 ± 3.61 mV in p.G279D/Kv7.3, -86.57 ± 4.71 mV in Kv7.2/p.G279D/Kv7.3 and -95.31 ± 4.63 mV in Kv7.2/Kv7.3WT, with a no significant difference between the groups ($p = 0.602$). Statistically significant differences are indicated by * $p < 0.05$, ** $p < 0.01$, *** $p < 0.001$, ns = no significant based on one-way ANOVA Tukey test.

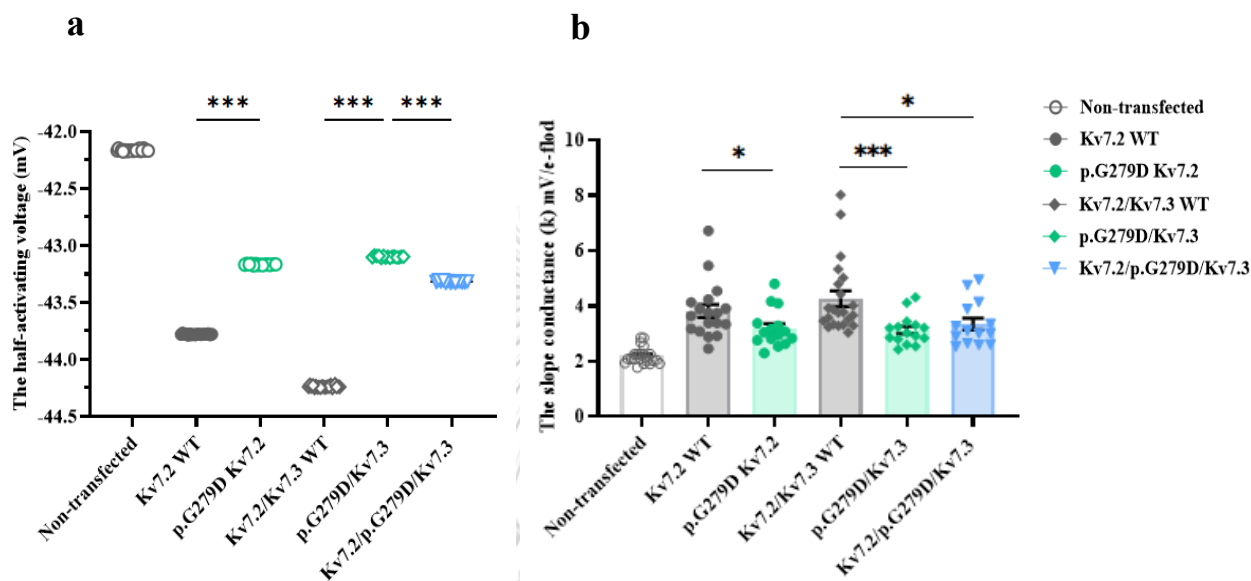


Figure 25 Comparison of K⁺ gating properties in homotetrameric and heterotetrameric p.G279D channels.

(a) The mean scores of the half-activating voltage ($V_{1/2}$) of homotetrameric channels were -43.17 ± 0.0013 mV in p.G279D Kv7.2 and -43.78 ± 0.0011 mV in Kv7.2WT, with a significant difference between the groups ($p < 0.001$). Post hoc analysis showed that the mean scores of p.G279D Kv7.2 channels was significantly increase when compared with Kv7.2WT ($p < 0.001$) while heterotetrameric channels were -43.01 ± 0.0018 mV in p.G279D/Kv7.3, -43.24 ± 0.0021 mV in Kv7.2/p.G279D/Kv7.3 and -44.24 ± 0.0019 mV in Kv7.2/Kv7.3WT, with a significant difference between the groups ($p < 0.001$). Post hoc analysis revealed significant increase when compared with Kv7.2/Kv7.3WT ($p < 0.001$ and $p < 0.001$, respectively) (b) The mean scores of the slope conductance (k) of homotetrameric channels were 3.19 ± 0.18 mV/e-fold in p.G279D Kv7.2 and 3.82 ± 0.24 mV/e-fold in Kv7.2WT, with a significant difference between the groups ($p < 0.001$). Post hoc analysis showed that the mean scores of p.G279D Kv7.2 channels was significantly decrease when compared with Kv7.2WT ($p < 0.001$) while heterotetrameric channels were 3.12 ± 0.14 mV/e-fold in p. G279D/Kv7.3, 3.34 ± 0.21 mV/e-fold in Kv7.2/p.G279D/Kv7.3 and 4.26 ± 0.28 mV/e-fold in Kv7.2/Kv7.3WT, with a significant difference between the groups ($p < 0.001$). Post hoc analysis revealed that the mean scores of p.G279D/Kv7.3 and Kv7.2/p.G279D/Kv7.3 channels were significantly decrease when compared with

Kv7.2Kv7.3WT ($p < 0.001$ and $p = 0.012$, respectively). Statistically significant differences are indicated by * $p < 0.05$, ** $p < 0.01$, *** $p < 0.001$, ns = no significant based on one-way ANOVA Tukey test.

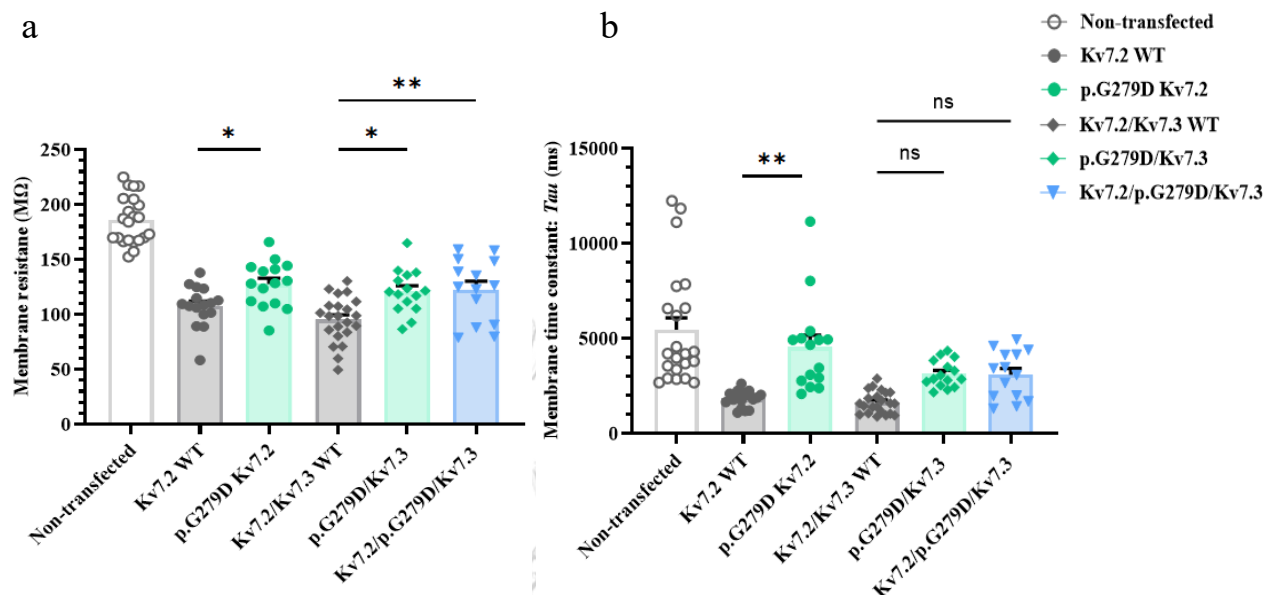


Figure 26 Comparison of the membrane resistance (R_m) and the membrane time constant (Tau) in homotetrameric and heterotetrameric of p.G279D channels.

(a) the mean scores of the membrane resistance (R_m) of homotetrameric channels were $127.69 \pm 3.38 \text{ M}\Omega$ in p.G279D Kv7.2 and $105.41 \pm 4.72 \text{ M}\Omega$ in Kv7.2WT, with a significant difference between the groups ($p < 0.001$). Post hoc analysis showed that the mean scores of p.G279D Kv7.2 expressed cells was significantly increase when compared with Kv7.2WT ($p = 0.034$) whereas heterotetrameric channels were $120.92 \pm 5.11 \text{ M}\Omega$ in p.G279D/Kv7.3, $122.64 \pm 7.61 \text{ M}\Omega$ in Kv7.2/p.G279D/Kv7.3 and $95.37 \pm 4.41 \text{ M}\Omega$ in Kv7.2/Kv7.3WT, with a significant difference between the groups ($p < 0.001$). Post hoc analysis revealed that the mean scores of p.G279D/Kv7.3 and Kv7.2/p.G279D/Kv7.3 expressed cells were significantly increase when compared with Kv7.2/Kv7.3WT expressed cells ($p = 0.01$ and $p = 0.006$, respectively). (b) the mean scores of the membrane time constant (Tau) of homotetrameric channels were $3859.70 \pm 254.93 \text{ ms}$ in p.G279D Kv7.2 and $1889.149 \pm 97.66 \text{ ms}$ in Kv7.2WT, with a significant difference between the groups ($p < 0.001$). Post hoc analysis showed that the mean scores of G279D expressed cells was significantly higher than in Kv7.2WT ($p = 0.008$) while, heterotetrameric channels were $3135.04 \pm 181.61 \text{ ms}$ in p.G279D/Kv7.3, $3092.34 \pm 334.87 \text{ ms}$ in Kv7.2/p.G279D/Kv7.3 and $1637.05 \pm 122.93 \text{ ms}$ in Kv7.2/Kv7.3WT, with a no significant difference between the groups ($p = 0.104$, $p = 0.138$, respectively). Statistically significant differences are indicated by * $p < 0.05$, ** $p < 0.01$, *** $p < 0.001$.

This result shows that the p.N258K and p.G279D reduced function of Kv.7.2 channels, as evidenced by the decrease in M-current, M-current density. There is also a loss of K⁺ gate properties with depolarization detection and reduced localization of p.N258K and p.G279D Kv7.2 leading to expression cells having an active Kv7.2 channel. The cell has increased membrane resistance. This also causes cells to spend more time changing their membrane potential. This is shown by the increase in the membrane time constant (*Tau*).



CHAPTER V DISCUSSION

Mutations in *KCNQ2* lead to infantile-onset epileptic disorders with broad severity spectrum from self-limited neonatal seizures to severe developmental and epileptic encephalopathy. More case reports might contribute to stronger genotype-phenotype found Thai patients with *KCNQ2*-related epilepsy, provide clinical and molecular characteristics, identify two novel genetic variants with functional studies. Both actually occur in the amino acid residues which have previously been reported. Nonetheless, different amino acid changes at the same amino acid residues may not have the same molecular pathomechanism. For example, the functional study of p.R213Q and p.R213W mutations in S4 have been showed a markedly reduced sensitivity to voltage, with p.R213Q lead to more severe functional changes than p.R213W. Additionally, the p.R213W phenotype caused benign familial neonatal convulsions (BFNC) and p.R213Q caused neonatal-onset epileptic encephalopathy (EE)⁶⁶.

The first novel genetic variant, p.N258K, found in patient 3 is a missense mutation in the S5-H5 linker. Because asparagine 258 is highly conserved sequence (SFLVYLAEKGENDHFDTYADAL) among homologous proteins in the voltage-gated K⁺ channel subunits⁶⁹. Asn 258 locate to the end of the pore or through the extracellular part of the pore (forming pores). This region may have conformational change during the depolarization and affect pore conductance and opening of the channel⁶⁹. This is supported by p.N258S mutation which effected trafficking of the mutation channel into the surface membrane that due to rearrange the structure within the pore region in the mutant protein⁴⁰. The findings of patch-clamp confirmed its pathogenicity; the M-current showed reducing current by almost ~40-50%, M-current density presented a reduction of about 50-55% indicating the dominant-negative effect on heterotetrameric channels, the current–voltage (I–V) curve showed reduce in conductance, K⁺ gating properties of channels; the half activating voltage ($V_{1/2}$) revealed depolarizing shift in voltage, increasing membrane resistance (R_m) and membrane time constant (Tau). The results agree with previous study, mutation of p.N258S have been reported functional defect; M-current reduced by almost 50%, the M-current density showed ~80 % reduction in homotetrameric channels and ~50 % reduction in heterotetrameric channels, the current–voltage (I–V) curve presented reduce in conductance, the half activating voltage ($V_{1/2}$) was slight depolarizing shift in

voltage⁴⁰. Other functional study in the S5-H5 linker of Kv7.2 protein subunits, p.A265P channels have been reported functional defect; M-current reduced by almost 20-40 %, , ~30-50 % reduction in M-current density in heterotetrameric, the current–voltage (I–V) curve showed reduce in conductance, the half activating voltage ($V_{1/2}$) was slight depolarizing shift in voltage⁴⁴. Both p.N258S and p.A265P mutations lead to loss-of-function and dominant-negative effect. So that, functional consequences of p.N258K effected loss-of-function dominant-negative effect of mutation.

The second novel genetic variant, p.G279D, found in patient 6 is missense mutation in pore-forming S5 and S6 region. Because Glycine 279 is highly conserved sequence (TIGGYGDK) in pore domain of the Kv7 channel family. Additionally, position Gly279 is GYG pore motif that is signature sequence of the selectivity filter (K⁺) and channel conductance and stability of the open pore state when there is a mutation in this location, it often leads to abnormal selectivity filter (K⁺) and protein expression. The findings of patch-clamp confirmed its pathogenicity; The M-current showed reducing almost 20-30%. The M-current density presented a reduction of about 50-55% indicating the weakly dominant-negative effect on heterotetrameric channels, the current–voltage (I–V) curve was showed decrease in conductance , K⁺ gating properties of channels; the half activating voltage ($V_{1/2}$) showed depolarizing shift in voltage, the membrane resistance (R_m) were increased. These results were supported by p.G279S mutation. It was loss-of-function that was only ~30-50% M-current was presented in the mutant channels and ~75% reduction of M-current density which have been expressed of dominant-negative effects on heterotetrameric channels^{32,67,70}. Other functional study in pore-forming S5 and S6 region. p.T274M and p.G290D mutation have been reported significant reduction of the current. The M-current density exhibited significant reduction of about ~30 to 50% which have been expressed of dominant-negative effects on heterotetrameric channels. So that, functional consequences of p.G279D mutation cause that a defect of channel permeability which lead to loss-of-function dominant-negative effect of mutation.

Although the p.N258K and p.G279D variant functional effect observed in the experimental model did not differ. The clinical outcome in the patient 3 and patient 6 differs greatly. Patient 3 has neonatal-onset seizures with normal developmental milestones at age one year and six months. The seizures were controlled after two anti-seizures medications. While

patient 6 has DEE phenotype. Previous studies have shown association between truncating variants and self-limited epilepsy.^{5,36} Complexity remains in the prediction of phenotype for *KCNQ2* missense variants. In vitro functional effect alone is no likely to explain the phenotype. Different factors including the variant locations and genetic modifier may also play important roles.

In conclusion, the findings confirmed functional characterization of p.N258K and p.G279D in different domains of the Kv7.2 subunits are loss-of-function defect as well as had dominant-negative effect of the mutants, that are pathogenic to infantile-onset epileptic disorders.



APPENDIX

Supplementary Table S1.....	53
Supplementary Table S2.....	54
Supplementary Table S3.	55
Supplementary Figure S1.....	56
Supplementary Figure S2.....	57
Supplementary Figure S3.	58



Supplementary Table S1. Clinical and molecular characteristics of nine patients with KCNQ2-related epilepsy

ID	Sex	Gestational birth	Family history	Seizure onset	Semiologies	EEG	Neuroimaging (age)	Antiepileptic drugs	Age at last visit	Outcome	NGS	Variant(s)	Reported (PMID)	Inheritance (allele from)	ACMG variant classification
1	F	Term	Neg	4 days	Spasms	NA	NA	VGB, TPM, PB, LEV, VPA	1 Y and 8 Mo	Severe GDD	WES-trio	c.601C>T (p.Arg201Cys)	Reported (25740509)	AD (<i>de novo</i>)	Pathogenic
2	F	Term	Neg	2 days	GT, sequential	Multifocal IED	MRI: unremarkable	LEV	9 Mo	Severe GDD	WES-trio	c.601C>T (p.Arg201Cys)	Reported (25740509)	AD (<i>de novo</i>)	Pathogenic
3	M	Term	Neg	3 days	Myoclonus eyes deviate left, head turn left	Multifocal IED	MRI: unremarkable (0 days)	Clonazepam	1 Y and 6 Mo	Normal inflexions	WES-trio	c.771C>G (p.Arg258Lys)	Novel	AD (<i>de novo</i>)	Pathogenic
4	F	Term (twin A, unaffected twin B)	Neg	2 days	GT	Suppression-burst	MRI: cerebral atrophy, corpus callosum agenesis (7 Mo)	PHT, PB, TPM, LEV, VGB, perampanel	2 Y and 9 Mo	Severe GDD	WGS-trio	c.821C>T (p Thr274Met)	Reported (24318194)	AD (<i>de novo</i>)	Pathogenic
5	F	Term	Neg	20 hrs	GT, Multifocal donic	Suppression-burst	CT: unremarkable	PB, LEV, TPM, perampanel	1 Y and 7 Mo	Severe GDD	WES-trio	c.821C>T (p Thr274Met)	Reported (24318194)	AD (<i>de novo</i>)	Pathogenic
6	F	Term	Neg	1 day	GT, sequential	Suppression-burst	MRI: unremarkable	PB, LEV, TPM, PHT, Clonazepam	3 Y and 5 Mo	Severe GDD	WES-trio	c.836G>A (p Gly279Asp)	Novel	AD (<i>de novo</i>)	Likely pathogenic
7	M	Term	Neg	36 hrs	GT	Multifocal IED	NA	LEV, PB	1 month	NA	WES-trio	c.881C>T (p Ala294Val)	Reported (26138355)	AD (<i>de novo</i>)	Pathogenic
8	F	Term	Neg	10 days	GT	Multifocal IED	MRI: cerebral atrophy (11 Mo)	LEV, TPM, diazepam	3 Y and 8 Mo	Severe GDD	WES-trio	c.1657C>T (p Arg553Trp)	Reported (23621294)	AD (<i>de novo</i>)	Pathogenic
9	M	Term	Neg	19 hrs	GT	Multifocal IED	MRI: unremarkable (2 weeks)	PB, TPM, LEV, CBZ	4 Mo	Bite bite contact not fix and	WES-trio	c.1687G>A (p Asp563Asn)	Reported (23621294)	AD (<i>de novo</i>)	Pathogenic

CBZ, carbamazepine; CT, computerized tomography; EEG, electroencephalogram; F, female; FLAIR, fluid attenuation inversion recovery; GDD, global developmental delay; GT, generalized tonic seizures;

GTc, generalized tonic clonic seizures; Hrs, hours; ID, identification; IED, interictal epileptiform discharges; LEV, Levetiracetam; LGA, large for gestational age; M, male; Mo, month; MRI, magnetic resonance imaging;

NA, not available; NCSE, nonconvulsive status epilepticus; Neg, negative; NGS, next-generation sequencing; PHT, pyridoxal-5-phosphate; PB, phenobarbital; PHT, phenytoin; SE, status epilepticus; T2W, T2-weighted imaging;

TPM, topiramate; VGB, vigabatrin; VPA, valproate; WES, whole-exome sequencing; WGS, whole-genome sequencing; Y, year (s)

Supplementary Table S2. Interpretation of the identified variants in the KCNQ2 gene

	Patient12	Patient3	Patient45	Patient6	Patient7	Patient8	Patient9
Variant†	c.601C>T (p.Arg201Cys)	c.774C>G (p.Ser258Ile)	cc.821C>T (p.Thr274Met)	c.836G>A (p.Gly279Asp)	c.881C>T (p.Ser294Val)	c.1657C>T (p.Arg553Trp)	c.1687G>A (p.Ser563Asn)
Inheritance	<i>De novo</i>	<i>De novo</i>	<i>De novo</i>	<i>De novo</i>	<i>De novo</i>	<i>De novo</i>	<i>De novo</i>
SIFT	D	D	D	D	D	D	D
PolyPhen-2	P.D.	P.D.	P.D.	P.D.	P.D.	P.D.	P.D.
M-CAP	P.P.	P.P.	P.P.	P.P.	P.P.	P.P.	P.P.
CADD	33	27.4	28.7	23.6	33	26.2	27.4
gnomAD	-	-	-	-	-	-	-
dbSNP	rs677503974	rs770187706	rs796052623	-	-	rs75584387	-
Evidence of pathogenicity	PS1, PS2, PM2	PS2, PM1, PM2, PMS, PP2	PS2, PS3, PM2	PS2, PM2, PP3	PS2, PM1, PM2, PP3, PPS	PS2, PM1, PM2, PP3, PPS	PS2, PM1, PM2, PP3, PPS
Classification‡	Pathogenic	Pathogenic	Pathogenic	Likely pathogenic	Pathogenic	Pathogenic	Pathogenic

D, deleterious; P.D., probably damaging; P.P., possibly pathogenic

SIFT, sorting intolerant from tolerant (<http://sift.jcvi.org>); PolyPhen-2, prediction of functional effects of human SNPs (<http://genetics.bwh.harvard.edu/pp2/>);

M-CAP, Mendelian clinically applicable pathogenicity score (<http://bejerano.stanford.edu/mcap>); CADD, combined annotation dependent depletion

(<https://cadd.gs.washington.edu>); recommended pathogenicity threshold >20; dbSNP (<https://www.ncbi.nlm.nih.gov/projects/SNP/>); gnomAD, <https://gnomad.broadinstitute.org>

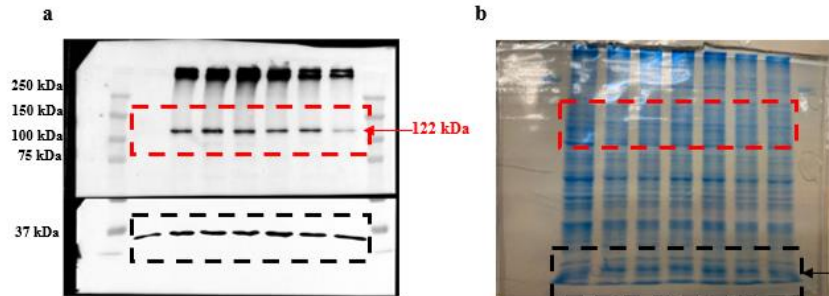
†NCBI (National Center of Biotechnology Information) reference sequence: NM_172107.4

‡According to the American College of Medical Genetics and Genomics interpretations guidelines (PMID 25741868)

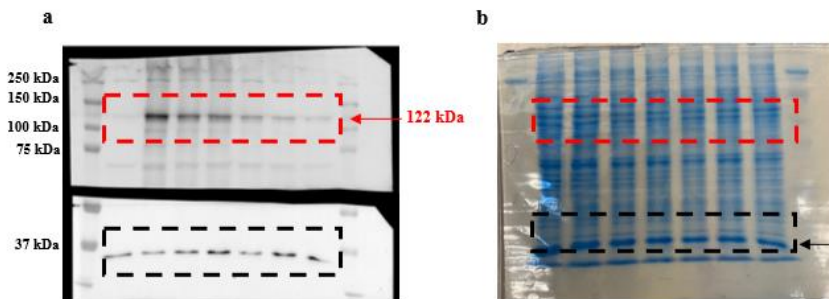
Supplementary Table S3. Electrophysiological parameter of currents recorded in HEK293 cells transfected with the indicated plasmid combinations

a							
	cDNA transfected (μg)	n	M-current at +50 mV (pA)	M-current density (pA/pF at +50 mV)	% reduction in M-current density		
Non-transfected	0	22	272.35 \pm 6.60	11.47 \pm 1.02			
Kv7.2 WT	2.5	18	498.71 \pm 29.27	28.02 \pm 1.81	100		
p.N258K/Kv7.2	2.5	15	374.52 \pm 13.83	***13.46 \pm 1.48	51.97		
p.G279D/Kv7.2	2.5	15	402.33 \pm 18.65	***14.19 \pm 1.03	49.36		
Kv7.2/Kv7.3WT	1.25:1.25	22	554.27 \pm 31.89	34.40 \pm 4.23	100		
p.N258K/Kv7.3	1.25:1.25	14	373.34 \pm 17.64	***15.79 \pm 1.83	54.09		
p.G279D/Kv7.3	1.25:1.25	15	424.10 \pm 18.36	***16.69 \pm 0.94	51.49		
Kv7.2/p.N258K/Kv7.3	0.625:0.625:1.25	13	385.26 \pm 18.44	***17.58 \pm 1.89	48.89		
Kv7.2/p.G279D/Kv7.3	0.625:0.625:1.25	14	431.91 \pm 30.52	***19.52 \pm 2.51	43.27		
b							
	cDNA transfected (μg)	n	V _{1/2} (mV) at -40 mV	k (mV/efold)	Membrane resistance (M Ω)	Membrane time constant (τ_{M}) (ms)	Reversal potential (mV)
Non-transfected	0	22	-42.16 \pm 0.0016	2.19 \pm 0.07	185.91 \pm 4.61	5452.62 \pm 640.36	-82.38 \pm 2.18
Kv7.2 WT	2.5	18	-43.78 \pm 0.0011	3.82 \pm 0.24	105.41 \pm 4.72	1889.149 \pm 97.66	-92.30 \pm 4.79
p.N258K/Kv7.2	2.5	15	*** -42.91 \pm 0.0013	* 2.93 \pm 0.15	** 135.65 \pm 4.21	**4550.06 \pm 621.66	-84.78 \pm 2.92
p.G279D/Kv7.2	2.5	15	*** -43.17 \pm 0.0013	* 3.19 \pm 0.18	* 127.69 \pm 3.38	***3859.70 \pm 254.93	-85.51 \pm 4.13
Kv7.2/Kv7.3WT	1.25:1.25	22	*** -44.24 \pm 0.0019	4.26 \pm 0.28	95.37 \pm 4.41	1637.05 \pm 122.93	-95.31 \pm 4.63
p.N258K/Kv7.3	1.25:1.25	14	*** -42.76 \pm 0.0021	***2.78 \pm 0.14	*** 137.32 \pm 5.59	** 3690 \pm 364.38	-89.83 \pm 3.94
p.G279D/Kv7.3	1.25:1.25	15	*** -43.01 \pm 0.0018	***3.12 \pm 0.14	* 120.92 \pm 5.11	3135.04 \pm 181.61	-90.33 \pm 3.61
Kv7.2/p.N258K/Kv7.3	0.625:0.625:1.25	13	*** -43.06 \pm 0.0017	**3.08 \pm 0.18	*** 133.06 \pm 5.78	*3337.08 \pm 418.03	-87.27 \pm 4.78
Kv7.2/p.G279D/Kv7.3	0.625:0.625:1.25	14	*** -43.24 \pm 0.0021	*3.34 \pm 0.21	** 122.64 \pm 7.61	3092.34 \pm 334.87	-89.78 \pm 4.77

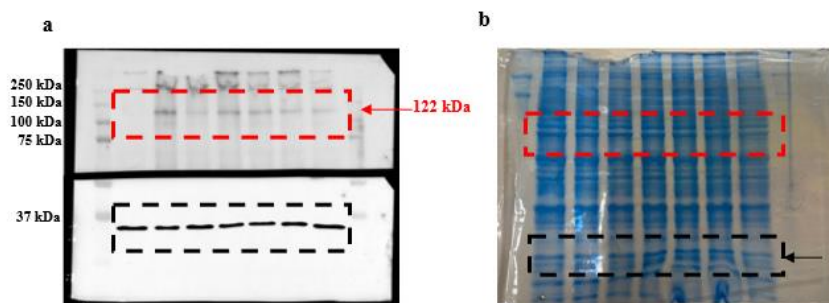
A. Total lysates



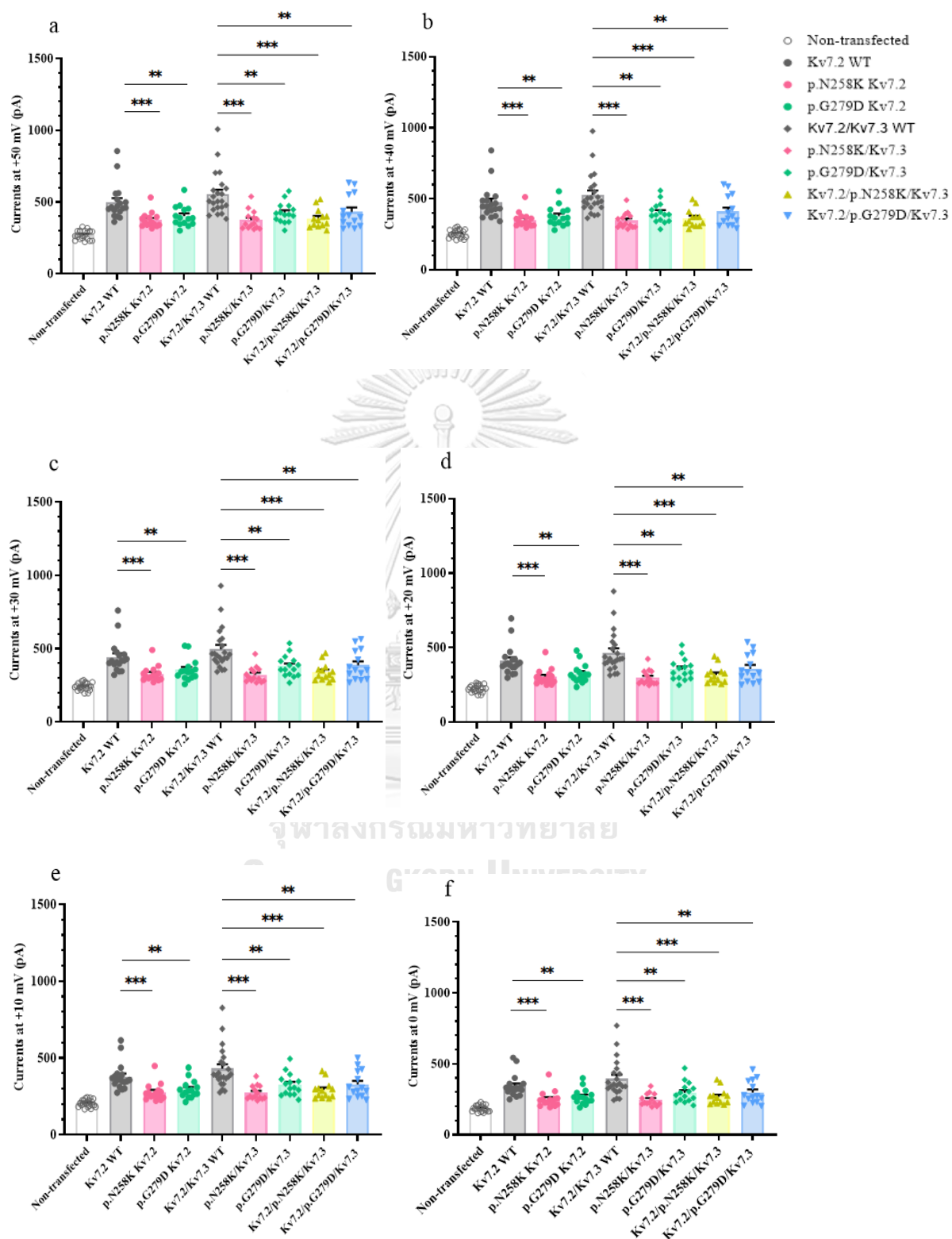
B. Membrane protein



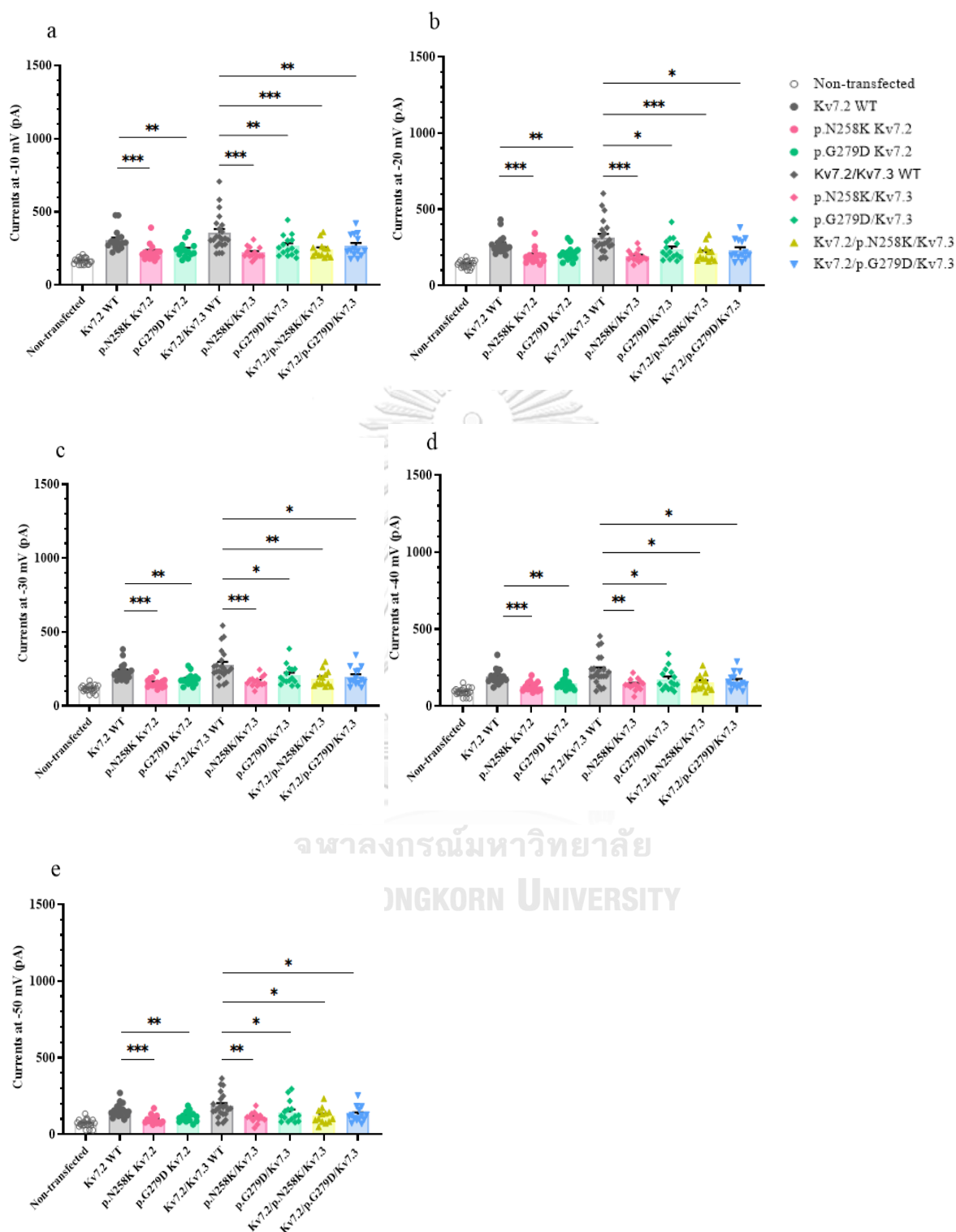
C. Cytoplasmic protein



Supplementary Figure S1. Original membranes (a) and gels (b) before cropping of dashed-line regions depicted in Figure 5 (A) Total lysate, (B) membrane protein fraction and (C) Cytoplasmic protein fraction. Red arrow indicates KCNQ2-GFP proteins (122 kDa) Black arrow indicates the GAPDH (37 kDa).



Supplementary Figure S3. Currents of mutant channels compared with WT at conditional voltage 0 mV to +50 mV. Statistically significant differences are indicated by * $p < 0.05$, ** $p < 0.01$, *** $p < 0.001$, ns = no significant based on one-way ANOVA Tukey test.



Supplementary Figure S4. Currents of mutant channels compared with WT at conditional voltage -50 mV to -10 mV. Statistically significant differences are indicated by * $p < 0.05$, ** $p < 0.01$, *** $p < 0.001$, ns = no significant based on one-way ANOVA Tukey test.

REFERENCES

- 1 Symonds, J. D. *et al.* Incidence and phenotypes of childhood-onset genetic epilepsies: a prospective population-based national cohort. *Brain* **142**, 2303-2318, doi:10.1093/brain/awz195 (2019).
- 2 Gaily, E., Lommi, M., Lapatto, R. & Lehesjoki, A. E. Incidence and outcome of epilepsy syndromes with onset in the first year of life: A retrospective population-based study. *Epilepsia* **57**, 1594-1601, doi:10.1111/epi.13514 (2016).
- 3 Stödberg, T. *et al.* Epilepsy syndromes, etiologies, and the use of next-generation sequencing in epilepsy presenting in the first 2 years of life: A population-based study. *Epilepsia* **61**, 2486-2499, doi:10.1111/epi.16701 (2020).
- 4 Wang, J. *et al.* Epilepsy-associated genes. *Seizure* **44**, 11-20, doi:10.1016/j.seizure.2016.11.030 (2017).
- 5 Goto, A. *et al.* Characteristics of KCNQ2 variants causing either benign neonatal epilepsy or developmental and epileptic encephalopathy. *Epilepsia* **60**, 1870-1880, doi:10.1111/epi.16314 (2019).
- 6 Singh, N. A. *et al.* KCNQ2 and KCNQ3 potassium channel genes in benign familial neonatal convulsions: expansion of the functional and mutation spectrum. *Brain* **126**, 2726-2737, doi:10.1093/brain/awg286 (2003).
- 7 Ronen, G. M., Rosales, T. O., Connolly, M., Anderson, V. E. & Leppert, M. Seizure characteristics in chromosome 20 benign familial neonatal convulsions. *Neurology* **43**, 1355-1360, doi:10.1212/wnl.43.7.1355 (1993).
- 8 Kalser, J. & Cross, J. H. The epileptic encephalopathy jungle - from Dr West to the concepts of aetiology-related and developmental encephalopathies. *Curr Opin Neurol* **31**, 216-222, doi:10.1097/wco.0000000000000535 (2018).
- 9 Nariai, H., Duberstein, S. & Shinnar, S. Treatment of Epileptic Encephalopathies: Current State of the Art. *J Child Neurol* **33**, 41-54, doi:10.1177/0883073817690290 (2018).
- 10 Orsini, A. *et al.* The role of inflammatory mediators in epilepsy: Focus on developmental and epileptic encephalopathies and therapeutic implications. *Epilepsy Res* **172**, 106588, doi:10.1016/j.eplepsyres.2021.106588 (2021).

- 11 Brown, D. A. & Passmore, G. M. Neural KCNQ (Kv7) channels. *Br J Pharmacol* **156**, 1185-1195, doi:10.1111/j.1476-5381.2009.00111.x (2009).
- 12 Sun, J. & MacKinnon, R. Cryo-EM Structure of a KCNQ1/CaM Complex Reveals Insights into Congenital Long QT Syndrome. *Cell* **169**, 1042-1050.e1049, doi:10.1016/j.cell.2017.05.019 (2017).
- 13 Cui, J. Voltage-Dependent Gating: Novel Insights from KCNQ1 Channels. *Biophys J* **110**, 14-25, doi:10.1016/j.bpj.2015.11.023 (2016).
- 14 Tsantoulas, C. & McMahon, S. B. Opening paths to novel analgesics: the role of potassium channels in chronic pain. *Trends Neurosci* **37**, 146-158, doi:10.1016/j.tins.2013.12.002 (2014).
- 15 Brown, D. A. & Adams, P. R. Muscarinic suppression of a novel voltage-sensitive K⁺ current in a vertebrate neurone. *Nature* **283**, 673-676, doi:10.1038/283673a0 (1980).
- 16 Zhang, J. *et al.* Identifying mutation hotspots reveals pathogenetic mechanisms of KCNQ2 epileptic encephalopathy. *Sci Rep* **10**, 4756, doi:10.1038/s41598-020-61697-6 (2020).
- 17 Millichap, J. J. *et al.* KCNQ2 encephalopathy: Features, mutational hot spots, and ezogabine treatment of 11 patients. *Neurol Genet* **2**, e96, doi:10.1212/nxg.0000000000000096 (2016).
- 18 Beghi, E. The Epidemiology of Epilepsy. *Neuroepidemiology* **54**, 185-191, doi:10.1159/000503831 (2020).
- 19 Guerrini, R. Epilepsy in children. *Lancet* **367**, 499-524, doi:10.1016/s0140-6736(06)68182-8 (2006).
- 20 Fisher, R. S. *et al.* ILAE official report: a practical clinical definition of epilepsy. *Epilepsia* **55**, 475-482, doi:10.1111/epi.12550 (2014).
- 21 Bhasin, H. & Sharma, S. The New International League Against Epilepsy (ILAE) 2017 Classification of Seizures and Epilepsy: What Pediatricians Need to Know! *Indian J Pediatr* **86**, 569-571, doi:10.1007/s12098-019-02910-x (2019).
- 22 Sander, J. W. Some aspects of prognosis in the epilepsies: a review. *Epilepsia* **34**, 1007-1016, doi:10.1111/j.1528-1157.1993.tb02126.x (1993).
- 23 Jensen, B. S. BMS-204352: a potassium channel opener developed for the treatment of stroke. *CNS Drug Rev* **8**, 353-360, doi:10.1111/j.1527-3458.2002.tb00233.x (2002).

- 24 Hedrich, U. B. S. *et al.* 4-Aminopyridine is a promising treatment option for patients with gain-of-function KCNA2-encephalopathy. *Sci Transl Med* **13**, eaaz4957, doi:10.1126/scitranslmed.aaz4957 (2021).
- 25 Fernandez-Marmiesse, A., Gouveia, S. & Couce, M. L. NGS Technologies as a Turning Point in Rare Disease Research , Diagnosis and Treatment. *Curr Med Chem* **25**, 404-432, doi:10.2174/0929867324666170718101946 (2018).
- 26 Salinas, V. *et al.* Clinical next generation sequencing in developmental and epileptic encephalopathies: Diagnostic relevance of data re-analysis and variants re-interpretation. *Eur J Med Genet* **64**, 104363, doi:10.1016/j.ejmg.2021.104363 (2021).
- 27 Hutchison, C. A., 3rd. DNA sequencing: bench to bedside and beyond. *Nucleic Acids Res* **35**, 6227-6237, doi:10.1093/nar/gkm688 (2007).
- 28 Green, E. D., Watson, J. D. & Collins, F. S. Human Genome Project: Twenty-five years of big biology. *Nature* **526**, 29-31, doi:10.1038/526029a (2015).
- 29 Zhang, J., Chiodini, R., Badr, A. & Zhang, G. The impact of next-generation sequencing on genomics. *J Genet Genomics* **38**, 95-109, doi:10.1016/j.jgg.2011.02.003 (2011).
- 30 Gokben, S. *et al.* Targeted next generation sequencing: the diagnostic value in early-onset epileptic encephalopathy. *Acta Neurol Belg* **117**, 131-138, doi:10.1007/s13760-016-0709-z (2017).
- 31 Tuchman, R. & Cuccaro, M. Epilepsy and autism: neurodevelopmental perspective. *Curr Neurol Neurosci Rep* **11**, 428-434, doi:10.1007/s11910-011-0195-x (2011).
- 32 Nappi, P. *et al.* Epileptic channelopathies caused by neuronal Kv7 (KCNQ) channel dysfunction. *Pflugers Arch* **472**, 881-898, doi:10.1007/s00424-020-02404-2 (2020).
- 33 Zara, F. *et al.* Genetic testing in benign familial epilepsies of the first year of life: clinical and diagnostic significance. *Epilepsia* **54**, 425-436, doi:10.1111/epi.12089 (2013).
- 34 Saitou, H. *et al.* Whole exome sequencing identifies KCNQ2 mutations in Ohtahara syndrome. *Ann Neurol* **72**, 298-300, doi:10.1002/ana.23620 (2012).
- 35 Weckhuysen, S. *et al.* Extending the KCNQ2 encephalopathy spectrum: clinical and neuroimaging findings in 17 patients. *Neurology* **81**, 1697-1703, doi:10.1212/01.wnl.0000435296.72400.a1 (2013).
- 36 Dirx, N., Miceli, F., Tagliatela, M. & Weckhuysen, S. The Role of Kv7.2 in

- Neurodevelopment: Insights and Gaps in Our Understanding. *Front Physiol* **11**, 570588, doi:10.3389/fphys.2020.570588 (2020).
- 37 Biervert, C. *et al.* A potassium channel mutation in neonatal human epilepsy. *Science* **279**, 403-406, doi:10.1126/science.279.5349.403 (1998).
- 38 Singh, N. A. *et al.* A novel potassium channel gene, KCNQ2, is mutated in an inherited epilepsy of newborns. *Nat Genet* **18**, 25-29, doi:10.1038/ng0198-25 (1998).
- 39 Schroeder, B. C., Kubisch, C., Stein, V. & Jentsch, T. J. Moderate loss of function of cyclic-AMP-modulated KCNQ2/KCNQ3 K⁺ channels causes epilepsy. *Nature* **396**, 687-690, doi:10.1038/25367 (1998).
- 40 Maljevic, S. *et al.* Temperature and pharmacological rescue of a folding-defective, dominant-negative KV 7.2 mutation associated with neonatal seizures. *Hum Mutat* **32**, E2283-2293, doi:10.1002/humu.21554 (2011).
- 41 Dedek, K. *et al.* Myokymia and neonatal epilepsy caused by a mutation in the voltage sensor of the KCNQ2 K⁺ channel. *Proc Natl Acad Sci U S A* **98**, 12272-12277, doi:10.1073/pnas.211431298 (2001).
- 42 Dedek, K., Fusco, L., Teloy, N. & Steinlein, O. K. Neonatal convulsions and epileptic encephalopathy in an Italian family with a missense mutation in the fifth transmembrane region of KCNQ2. *Epilepsy Res* **54**, 21-27, doi:10.1016/s0920-1211(03)00037-8 (2003).
- 43 Miceli, F. *et al.* Genotype-phenotype correlations in neonatal epilepsies caused by mutations in the voltage sensor of K(v)7.2 potassium channel subunits. *Proc Natl Acad Sci U S A* **110**, 4386-4391, doi:10.1073/pnas.1216867110 (2013).
- 44 Orhan, G. *et al.* Dominant-negative effects of KCNQ2 mutations are associated with epileptic encephalopathy. *Ann Neurol* **75**, 382-394, doi:10.1002/ana.24080 (2014).
- 45 Yellen, G. The voltage-gated potassium channels and their relatives. *Nature* **419**, 35-42, doi:10.1038/nature00978 (2002).
- 46 Chapman, M. L., Krovetz, H. S. & VanDongen, A. M. GYGD pore motifs in neighbouring potassium channel subunits interact to determine ion selectivity. *J Physiol* **530**, 21-33, doi:10.1111/j.1469-7793.2001.0021m.x (2001).
- 47 Haitin, Y. & Attali, B. The C-terminus of Kv7 channels: a multifunctional module. *J Physiol* **586**, 1803-1810, doi:10.1113/jphysiol.2007.149187 (2008).

- 48 Choveau, F. S. & Shapiro, M. S. Regions of KCNQ K(+) channels controlling functional expression. *Front Physiol* **3**, 397, doi:10.3389/fphys.2012.00397 (2012).
- 49 Schroeder, B. C., Hechenberger, M., Weinreich, F., Kubisch, C. & Jentsch, T. J. KCNQ5, a novel potassium channel broadly expressed in brain, mediates M-type currents. *J Biol Chem* **275**, 24089-24095, doi:10.1074/jbc.M003245200 (2000).
- 50 McCoy, J. G. & Nimigean, C. M. Structural correlates of selectivity and inactivation in potassium channels. *Biochim Biophys Acta* **1818**, 272-285, doi:10.1016/j.bbamem.2011.09.007 (2012).
- 51 So, I., Ashmole, I., Davies, N. W., Sutcliffe, M. J. & Stanfield, P. R. The K⁺ channel signature sequence of murine Kir2.1: mutations that affect microscopic gating but not ionic selectivity. *J Physiol* **531**, 37-50, doi:10.1111/j.1469-7793.2001.0037j.x (2001).
- 52 Soldovieri, M. V., Miceli, F. & Tagliatalata, M. Driving with no brakes: molecular pathophysiology of Kv7 potassium channels. *Physiology (Bethesda)* **26**, 365-376, doi:10.1152/physiol.00009.2011 (2011).
- 53 Greene, D. L. & Hoshi, N. Modulation of Kv7 channels and excitability in the brain. *Cell Mol Life Sci* **74**, 495-508, doi:10.1007/s00018-016-2359-y (2017).
- 54 Soldovieri, M. V. *et al.* Early-onset epileptic encephalopathy caused by a reduced sensitivity of Kv7.2 potassium channels to phosphatidylinositol 4,5-bisphosphate. *Sci Rep* **6**, 38167, doi:10.1038/srep38167 (2016).
- 55 Lek, M. *et al.* Analysis of protein-coding genetic variation in 60,706 humans. *Nature* **536**, 285-291, doi:10.1038/nature19057 (2016).
- 56 Piccolino, M. Animal electricity and the birth of electrophysiology: the legacy of Luigi Galvani. *Brain Res Bull* **46**, 381-407, doi:10.1016/s0361-9230(98)00026-4 (1998).
- 57 Hamill, O. P., Marty, A., Neher, E., Sakmann, B. & Sigworth, F. J. Improved patch-clamp techniques for high-resolution current recording from cells and cell-free membrane patches. *Pflugers Arch* **391**, 85-100, doi:10.1007/bf00656997 (1981).
- 58 Hodgkin, A. L. & Huxley, A. F. A quantitative description of membrane current and its application to conduction and excitation in nerve. *J Physiol* **117**, 500-544, doi:10.1113/jphysiol.1952.sp004764 (1952).
- 59 Jun, J. J. *et al.* Fully integrated silicon probes for high-density recording of neural activity.

- Nature* **551**, 232-236, doi:10.1038/nature24636 (2017).
- 60 Kornreich, B. G. The patch clamp technique: principles and technical considerations. *J Vet Cardiol* **9**, 25-37, doi:10.1016/j.jvc.2007.02.001 (2007).
- 61 Brock, L. G., Coombs, J. S. & Eccles, J. C. The recording of potentials from motoneurons with an intracellular electrode. *J Physiol* **117**, 431-460, doi:10.1113/jphysiol.1952.sp004759 (1952).
- 62 Kwan, P. *et al.* Definition of drug resistant epilepsy: consensus proposal by the ad hoc Task Force of the ILAE Commission on Therapeutic Strategies. *Epilepsia* **51**, 1069-1077, doi:10.1111/j.1528-1167.2009.02397.x (2010).
- 63 Shotelersuk, V. *et al.* The Thai reference exome (T-REx) variant database. *Clin Genet* **100**, 703-712, doi:10.1111/cge.14060 (2021).
- 64 Richards, S. *et al.* Standards and guidelines for the interpretation of sequence variants: a joint consensus recommendation of the American College of Medical Genetics and Genomics and the Association for Molecular Pathology. *Genet Med* **17**, 405-424, doi:10.1038/gim.2015.30 (2015).
- 65 Kaur, J., Nygren, A. & Vigmond, E. J. Fitting membrane resistance along with action potential shape in cardiac myocytes improves convergence: application of a multi-objective parallel genetic algorithm. *PLoS One* **9**, e107984, doi:10.1371/journal.pone.0107984 (2014).
- 66 Isokawa, M. Membrane time constant as a tool to assess cell degeneration. *Brain Res Brain Res Protoc* **1**, 114-116, doi:10.1016/s1385-299x(96)00016-5 (1997).
- 67 Peters, H. C., Hu, H., Pongs, O., Storm, J. F. & Isbrandt, D. Conditional transgenic suppression of M channels in mouse brain reveals functions in neuronal excitability, resonance and behavior. *Nat Neurosci* **8**, 51-60, doi:10.1038/nn1375 (2005).
- 68 Jiang, B., Sun, X., Cao, K. & Wang, R. Endogenous Kv channels in human embryonic kidney (HEK-293) cells. *Mol Cell Biochem* **238**, 69-79, doi:10.1023/a:1019907104763 (2002).
- 69 Yalçın, O. *et al.* A novel missense mutation (N258S) in the KCNQ2 gene in a Turkish family afflicted with benign familial neonatal convulsions (BFNC). *Turk J Pediatr* **49**, 385-389 (2007).

- 70 Sharawat, I. K., Kasinathan, A., Sahu, J. K. & Sankhyan, N. Response to Carbamazepine in KCNQ2 Related Early Infantile Epileptic Encephalopathy. *Indian J Pediatr* **86**, 301-302, doi:10.1007/s12098-018-2796-8 (2019).





จุฬาลงกรณ์มหาวิทยาลัย
CHULALONGKORN UNIVERSITY

VITA

NAME Suphalak Chokvithaya

DATE OF BIRTH 5 April 1983

PLACE OF BIRTH Bangkok

INSTITUTIONS ATTENDED Faculty of Medicine, Chulalongkorn University

HOME ADDRESS 5/3 Soi Pracha Uthit 76 Intersection 8, Thung Khru Subdistrict,
Thung Khon District, Bangkok

PUBLICATION -

AWARD RECEIVED -

